

Impact of changes in climate and CO₂ on the carbon storage potential of vegetation under limited water availability using SEIB-DGVM version 3.02

Shanlin Tong^{1,2,3}, Weiguang Wang^{2,3*}, Jie Chen^{1,*}, Chong-Yu Xu⁴, Hisashi Sato⁵, Guoqing Wang⁶

¹State Key Laboratory of Water Resources and Hydropower Engineering Science, Wuhan University, Wuhan, 430072, Peoples R China

²State Key Laboratory of Hydrology-Water Resources and Hydraulic Engineering, Hohai University, Nanjing, 210098, Peoples R China

³College of Hydrology and Water Resources, Hohai University, Nanjing, 210098, Peoples R China

⁴Department of Geosciences, University of Oslo, Oslo, N-0316, Norway

⁵Japan Agency for Marine-Earth Science and Technology, Yokohama, 236-0001, Japan

⁶Nanjing Hydraulic Research Institute, Nanjing, 210029, Peoples R China

*Correspondence to: Weiguang Wang (wangweiguang2016@126.com); Jie Chen (jiechen@whu.edu.cn)

Abstract

Documenting year-to-year variations in carbon storage potential in terrestrial ecosystems is crucial for the determination of carbon dioxide (CO₂) emissions. However, the magnitude, pattern and inner biomass partitioning of carbon storage potential, and the effect of the changes in climate and CO₂ on inner carbon stocks, remain poorly quantified. Herein, we use a spatially explicit individual based-dynamic global vegetation model to investigate the influences of the changes in climate and CO₂ on the enhanced carbon storage potential of vegetation. The modelling included a series of factorial simulations using the CRU dataset from 1916 to 2015. The results show that CO₂ predominantly leads to a persistent and widespread increase in light-gathering vegetation biomass carbon stocks (~~GVBC~~LVBC) and water-gathering vegetation biomass carbon stocks (WVBC). Climate change appears to play a secondary role in carbon storage potential. Importantly, with the intensification of water stress, the magnitude of the light- and water-gathering responses in vegetation carbon stocks gradually decreases. Plants adjust carbon allocation to decrease the ratio between ~~GVBC~~LVBC and WVBC for capturing more water. Changes in the pattern of vegetation carbon storage was linked to zonal limitations in water, which directly weakens and indirectly regulates the response of potential vegetation carbon stocks to a changing environment. Our findings differ from previous modelling evaluations of vegetation that ignored inner carbon

32 dynamics and demonstrates that the long-term trend in increased vegetation biomass carbon stocks is
33 driven by CO₂ fertilization and temperature effects that are controlled by water limitations.

34 **1 Introduction**

35 As a result of the changes in climate and atmospheric carbon dioxide (CO₂), the terrestrial ecosystem
36 carbon cycle exhibits remarkable trends in interannual variations, which induce uncertainty in estimated
37 carbon budgets (Erb et al., 2018; Keenan et al., 2017). Recent studies assessing interannual fluctuations
38 in terrestrial carbon sinks have shown that the land carbon cycle is the most uncertain component of the
39 global carbon budget (Ahlstrom et al., 2015; Piao et al., 2020; Jung et al., 2017; Humphrey et al., 2018;
40 Gentine et al., 2019; Humphrey et al., 2021). These uncertainties result from an incomplete understanding
41 of vegetation biomass carbon production, allocation, storage, loss, and turnover time (Bloom et al., 2016).
42 The extent and distribution of vegetation carbon storage is central to our understanding of how to
43 maintain a balanced land carbon cycle. Changes in terrestrial vegetation carbon storage have a significant
44 effect on atmospheric CO₂ concentrations and determine whether biomes become a source or sink of
45 carbon (Erb et al., 2018; Humphrey et al., 2018; Terrer et al., 2021). Therefore, investigating the
46 processes producing changes in carbon storage is key to improving the accuracy of estimated terrestrial
47 carbon budgets, and to tap the greenhouse-gas moderation potentials of vegetation (Ipcc, 2007; Roy et
48 al., 2001).

49

50 The atmospheric CO₂ concentration ~~are is~~ affected by the vegetation carbon stock, while the long-term
51 trend of vegetation carbon storage capacity is also affected by the changes in climate and CO₂. Since the
52 beginning of industrialization, there has been a noticeable enhancement in the plant capacity of storing
53 and sequestering carbon, which is needed for stabilizing greenhouse gas concentrations and mitigating
54 global warming (Chen et al., 2019; Pan et al., 2011; Le Noë et al., 2020; Magerl et al., 2019; Bayer et al.,
55 2015; Harper et al., 2018). Due to the interaction between terrestrial vegetation and a changing
56 environment, both photosynthesis and respiration of the vegetation also changed. To better absorb CO₂
57 and sunlight required for photosynthesis, vegetated zones are gradually covered by vegetation with
58 higher plant height and wider leaf area (Erb et al., 2008).—This change has coincided with a widespread
59 change in other vegetation features, including a positive increase in annual gross primary productivity

60 and a greening of the biosphere (Madani et al., 2020; Zhu et al., 2016). The spatiotemporal distribution
61 and environmental drivers in total carbon storage potential have been well documented on the basis of
62 model estimates and satellite-based assessments (Erb et al., 2007; Erb et al., 2018; Bazilevich et al., 1971;
63 Saugier et al., 2001; Bartholome and Belward, 2005; Olson et al., 1983; Pan et al., 2013; Ajtay et al.,
64 1979; Ruesch and Gibbs, 2008; Kaplan et al., 2011; Shevliakova et al., 2009; Prentice et al., 2011; West
65 et al., 2010; Hurtt et al., 2011). In contrast, the variability of inner components of carbon storage potential
66 has not been extensively studied. Without an accurate assessment of the dynamics of each fraction,
67 attribution of carbon storage potential to environmental drivers is highly uncertain. Consequently,
68 partitioning potential vegetation carbon storage and revealing its inner processes are essential to
69 accurately comprehend the current state of carbon storage capacity and reveal the influence of various
70 drivers on the long-term trend of carbon storage potential.

71

72 The change of carbon storages in vegetation inner components is not only affected by environmental
73 factors, but also controlled by allocation scheme of assimilated carbon. Fractional dynamics of the carbon
74 stock are widely used as a key indicator to investigate the responses of vegetation to environmental
75 drivers, which also reflect the response strategies of vegetation in environments with different water
76 limitations (Yang et al., 2010). In arid regions, vegetation utilizes a tolerance strategy to allocate biomass,
77 storing more biomass carbon in roots to resist enhanced water stress (Chen et al., 2013). Conforming to
78 the optimal partitioning hypothesis, plants store more carbon in shoots and leaves in environments where
79 water is more available and shift more carbon to roots when water is more limited (Yang et al., 2010;
80 McConnaughay and Coleman, 1999). Water availability controls both carbon allocation and storage and
81 can potentially transform zones characterized by a positive response to changes in climate and CO₂ to
82 zones exhibiting a negative response. For example, global warming positively stimulates plant
83 productivity (Keenan et al. 2017)~~For example, global warming stimulates plant productively, while~~
84 Madani et al. (2020) found that plants productively with water stress show a negative response to
85 temperature rise in tropical zones. With increased warming, water limitations are ~~predictable-predicted~~
86 to increasingly reduce the proportion of leaves' biomass, and decrease plant photosynthesis (Ma et al.,
87 2021). Water limitations have a strong regulating effect on the spatial pattern of change in vegetation
88 carbon storage, demonstrating the effects of the changes in climate and CO₂ on the dynamics of the plant

89 organs are affected by the terrestrial water gradient. Thus, it is important to systematically investigate
90 the distinct responses of carbon storage potential to changes in climate and CO₂ under differing
91 conditions of water stress.

92

93 As documented above, many studies have investigated the total changes in zonal and global terrestrial
94 storage of carbon, while few studies have examined trends in the components partitioning of vegetation
95 carbon storage. Large gaps in our knowledge of the effects of various drivers on the partitioning of carbon
96 stocks in vegetation biomass remain. Meanwhile, plants adjust carbon allocation scheme to adapt to
97 environmental change. With increased warming, an increase in the magnitude of water stress may
98 dramatically change or even reverse the impact of these drivers on inner components of carbon storage
99 (Ma et al., 2021). Evaluating the response pattern of carbon stocks to various drivers under conditions of
100 limited water is elemental for clearly documenting the response mechanism of vegetation carbon storage
101 potential.

102

103 Here, we use a spatially explicit individual-based dynamic global vegetation model (SEIB-DGVM),
104 along with the components partitioning method to (1) systematically determine the long-term variability
105 of carbon storage potential and understand its response mechanisms, and (2) estimate trends in
106 partitioning of potential biomass carbon stocks of vegetation biomass. Throughout this study, the
107 potential biomass carbon stock, biomass carbon stored in vegetation without anthropogenic disturbance,
108 is recognized as ~~an indicator~~an indicator proxy of the potential of carbon storage by natural vegetation. Using a set
109 of factorial simulations to isolate responses to environmental change, we analyse the contributions of
110 multiple driving factors to the trends of two fractions of carbon stock at large scales individually. We
111 then conceptualize the role of water availability through an aridity index (AI), in which hydrological
112 zones are subdivided by their degree of aridity. By comparing the differences in the magnitude of
113 response between the fractions of light- and water-gathering carbon stocks for varying degrees of water
114 availability, we assess the effect of water limitations on the response pattern of potential carbon stocks
115 to changes in climate and CO₂.

116 **2 Model description, experimental design, observational data, and evaluation metrics**

117 In this section, we provided a list of data source (Sect. 2.1), an overview of the modelling concept (Sect.
118 2.2), the representation of biomass carbon stock partitioning in the SEIB-DGVM (Sect. 2.3), an overview
119 of the experimental scheme used in the model simulations (Sect. 2.4), and an overview about data source
120 and pre-processing of observation dataset for model evaluation (Sect. 2.5).

121 **2.1 Forcing Data**

122 Long-term daily meteorological time-series data are required to run model simulations, including
123 precipitation, daily range of air temperature, mean daily air temperature, downward shortwave radiation
124 at midday, downward longwave radiation at midday, wind velocity, and relative humidity. These data
125 were obtained from the Climatic Research Unit (CRU) time series 4.00 gridded dataset (degree 0.5°) for
126 the period 1901–2015 (Harris et al., 2020). Because the CRU dataset is a monthly based dataset, the
127 monthly meteorological data were converted into daily climatic variables by supplementing daily
128 climatic variability within each month using the National Centre for Environmental Prediction (NCEP)
129 daily climate dataset. The NCEP data, displayed using the T62 Gaussian grid with 192×94 points, was
130 interpolated into a 0.5° grid (which corresponds to the CRU dataset) using a linearly interpolation method.
131 By combining the CRU data, with the interpolated NCEP dataset, we were able to directly obtain the
132 most of driving meteorological data (details in Sato et al. (2020)). Neither the CRU nor NCEP datasets
133 included downward shortwave and longwave radiation at midday. Thus, daily cloudiness values in the
134 NCEP were used to calculate radiation values using empirical functions (Sato et al., 2007). These data
135 were all aggregated to a daily timescale with 0.5° resolution to run SEIB-DGVM.

136

137 Atmospheric CO₂ concentrations were collected from Sato et al. (2020), which contains reconstructed
138 CO₂ concentrations between 1901 and 2015. The statistical reconstruction of global atmospheric CO₂
139 was used in this analysis. These reconstructions were based on present annual CO₂ concentrations
140 recorded from the Mauna Loa monitoring station. These data assume atmospheric CO₂ concentration
141 was 284 ppm in 1750, and statistically interpolates atmospheric CO₂ concentrations to fill the gap from
142 1750 to 2015.

143

144 The physical parameters of the soil used in the model include soil moisture at the saturation point, field
145 capacity, matrix potential, wilting point and albedo. These data were obtained from the Global Soil
146 Wetness Project 2.

147 **2.2 Overview of modelling concept in SEIB-DGVM**

148 Model SEIB-DGVM version 3.02 (Sato et al., 2020) was employed in this study. This is a process-based
149 dynamic global vegetation model driven by meteorological and soil data. It is an explicit and
150 computationally efficient carbon cycle model designed to simulate transient effects of environmental
151 change on terrestrial ecosystems and land-atmosphere interactions. It describes three groups of processes:
152 land-based physical processes (e.g., hydrology, radiation, aridity), plant physiological processes (e.g.,
153 photosynthesis, respiration, litter), and plant dynamic processes (e.g., establishment, growth, mortality).
154 Twelve plant functional types (PFTs) were classified. During the simulation, a sample plot was
155 established at each grid box, and then the growth, competition, and mortality of each the individual PFTs
156 within each plot were modelled by considering the specify conditions for that individual as it relates to
157 other individuals that surround it (Sato et al., 2007).

158

159 SEIB-DGVM treats the relationships between soil, atmosphere, and terrestrial biomes in a consistent
160 manner, including the fluxes of energy, water, and carbon. Based on specified climatic conditions and
161 soil properties, SEIB-DGVM simulates the carbon cycle, energy balance, and hydrological processes.
162 SEIB-DGVM utilizes three computational time steps: (1) During the growth phase, the metabolic
163 procedures including photosynthesis, respiration, and carbon allocation are executed for each individual
164 tree every simulation day. (2) The monthly process of tree growth including reproduction, trunk growth,
165 and expansion of a cross-sectional area of the crown are executed. (3) On the last day of each year, the
166 height of the lowest branch increases as a result of purging crown disks, or self pruning of branches, at
167 the bottom of the crown layer. The simulated unit of the model is a 30 m × 30 m spatially explicit ‘virtual
168 forest’. A grass layer was placed under the woody layer, and provides for a comprehensive, spatially
169 explicit quantification of terrestrial carbon sinks and sources. The soil depth was set at 2 m and was
170 divided into 20 layers, each with a thickness of 0.1 m. The photosynthetic rate of a single-leaf was
171 simulated following a Michaelis-type function (Ryan, 1991). Respiration was divided into two types:
172 growth respiration and maintenance respiration. Growth respiration is defined as a construction cost for

173 plant biosynthesis, which is quantified by the chemical composition of each organ (Poorter, 1994).
174 Maintenance respiration of live plants occurs every day regardless of the phenological phase, and is
175 controlled by the temperature and nitrate content of each organ (Ryan, 1991). For a wide variety of plant
176 organs, the maintenance respiration rate is linearly related to the nitrogen content of living tissue. The
177 relative proportions of nitrogen in each organ for any PFT are linearly correlated. N-deposition ~~doesn't~~
178 isn't included -in SEIB-DGVM. Atmospheric CO₂ was envisioned to be absorbed by photosynthesis of
179 woody PFTs and grass PFTs. This assimilated carbon flux was then allocated into all the plant organs
180 (leaf, trunk, root, and stock), where maintenance respiration and growth respiration occur. The hydrology
181 module treats precipitation, canopy interception, transpiration, evaporation, meltwater, and penetration.

182 **2.3 Carbon stock of vegetation biomass partitioning**

183 **2.3.1 Parameterization of daily allocation**

184 Flexible allocation schemes about resources and biomass are set up in the framework of the SEIB-DGVM
185 biogeochemical model. Based on the updated observation data, the allocation schemes of Boreal Needle-
186 leaved summer-green trees and Tropical Broad-leaved evergreen trees ~~were~~ are improved at SEIB-
187 DGVM V3.02. Allocation schemes of other PFTs are the same as the original version. Atmospheric CO₂
188 is assimilated by the photosynthesis of both woody and grass foliage, and then is added into the non-
189 structural carbon of the plant. This non-structural carbon of photosynthetic production is allocated to all
190 the plant organs (foliage, trunk, root, and stock), supplying what is needed for the maintenance and
191 growth of each organ. When the non-structural carbon is greater than 0 during the growth phase, the
192 following dynamic carbon allocation is executed for each individual plant at the daily time scale, such
193 that:

194 (1) When the fine root biomass ($mass_{root}$) of wood or grass does not satisfy minimum requirements for
195 fulfilling functional balance ($mass_{leaf}/FR_{ratio}$), the mass of non-structural carbon is allocated to the root
196 biomass to supplement the deficit. Here, $mass_{leaf}$ is the leaf biomass, and FR_{ratio} is the ratio of $mass_{leaf}$ to
197 $mass_{root}$ satisfying the functional balance.

198 (2) The stock biomass is supplemented until it is equal to leaf biomass. This scheme is active after the
199 first thirty days of the growing phase.

200 (3) Woody leaf biomass is constrained by three limitations of the maximum leaf biomass, which are

201 calculated as follows:

$$202 \quad max_1 = (crown_{area} + \pi crown_{diameter} crown_{depth}) \frac{LA_{max}}{SLA} \quad (1)$$

$$203 \quad max_2 = ALM_1 \frac{\pi (dbh_{heartwood}/2 + dbh_{sapwood}/2)^2 - \pi (dbh_{heartwood}/2)^2}{SLA} \quad (2)$$

$$204 \quad max_3 = \frac{mass_{available}}{RG_f} \quad (3)$$

$$205 \quad mass_{leaf} = \min(max_1, max_2, max_3) \quad (4)$$

206 where max_1 , max_2 , and max_3 are, respectively, maximum leaf biomass for a given crown surface
207 area, cross-sectional area of sapwood, and non-structural carbon; SLA is a constant of PFTs leaf area
208 ($m^2 g^{-1}$); LA_{max} is the plant functional type specific maximum leaf area per unit crown surface area
209 excluding the bottom soffit layer ($m^2 m^{-2}$); ALM_1 represents the area of transport tissue per unit biomass,
210 and is a constant (dimensionless). If the $mass_{leaf}$ is less than the minimum (max_1, max_2, max_3), the
211 mass of non-structural carbon is allocated into leaf biomass to supplement the deficit.

212 When the leaf area index of grass equals the optimal leaf area index, it stops to allocate non-structural
213 carbon to grass leaf, which is calculated as:

$$214 \quad lai_{opt} = \frac{\ln par_{grass} - \ln \left\{ \frac{p_{sat}}{lue} \left[\left(1 - \frac{cost/SLA}{0.09093 \times dlen \times p_{sat}} \right)^{-2} - 1 \right] \right\}}{eK} \quad (5)$$

215 where lai_{opt} is the optimal leaf area index ($m^2 m^{-2}$); par_{grass} is the grass photosynthetically active
216 radiation ($\mu mol \text{ photon } m^{-2} s^{-1}$); p_{sat} is the light-saturated photosynthetic rate ($\mu CO_2 m^{-2} s^{-1}$); lue is
217 the light-use efficiency of photosynthesis ($mol CO_2 mol \text{ photon}^{-1}$); $cost$ is the cost of maintaining
218 leaves per unit leaf mass per day ($g DM g DM^{-1} day^{-1}$); $dlen$ is day length (hour); and eK is light
219 attenuation coefficient at midday.

220 (4) When non-structural carbon is less than 10 g dry mass (DM) PFT^{-1} or annual NPP is less than 10 g
221 DM PFT^{-1} in the previous year, the following daily simulation processes (5-6) will be skipped.

222 (5) When total woody biomass is more than 10 kg DM, which defines the minimum tree size for
223 reproduction, ~~This~~ 10% NSC-non-structural carbon is used for every daily process of reproduction,
224 including having flowers, pollen, nectar, fruits, and seeds. These organs are not explicitly modelled in
225 SEIB-DGVM.

226 (6) During the simulation of trunk growth, the remaining non-structural carbon is allocated to sapwood
227 biomass. There is no direct allocation to heartwood, which is transformed slowly from sapwood biomass.
228 For grass PFTs biomass, the densities of all organs comprising the biomass never decline below 0.1 g

229 DM m⁻² even if the environment is deteriorated for grass survival. A more detailed description of SEIB-
 230 DGVM is given by Sato et al. (2007).

231

232 To control plant phenology and the rate of photosynthesis as a function of the limitation in terrestrial
 233 water, the physiological status of the limitation of terrestrial water is calculated as:

$$234 \quad p_{sat} = PMAX ce_{tmp} ce_{co_2} ce_{water} \quad (6)$$

$$235 \quad ce_{water} = \sqrt{stat_{water}} \quad (7)$$

$$236 \quad stat_{water} = \frac{\max(pool_{w(1)}/Depth_{(1)}, pool_{w(2)}/Depth_{(2)}) - W_{wilt}}{W_{fi} - W_{wilt}} \quad (8)$$

237 where p_{sat} is the single-leaf photosynthetic rate of tree PFTs and grass PFTs ($\mu\text{mol CO}_2 \text{ m}^{-2} \text{ s}^{-1}$);
 238 $PMAX$ is the potential maximum of photosynthetic rate ($\mu\text{mol mol}^{-1} \text{ CO}_2 \text{ m}^{-2} \text{ s}^{-1}$); ce_{tmp} and ce_{co_2} are
 239 the temperature and CO₂ concentration effect coefficient (dimensionless), separately; ce_{water} is the
 240 water effect coefficient (dimensionless); $stat_{water}$ is the physiological status of the terrestrial water
 241 limitation, which ranges between 0.0–1.0, dimensionless; $pool_{w(n)}$ is the water content in soil layer n,
 242 mm; $Depth_{(n)}$ is the depth of the soil layer n, mm; W_{wilt} is soil moisture at the wilting point, m⁻¹;
 243 and W_{fi} is soil moisture at field capacity, m⁻¹. When the temperature of all soil layers is less than 0°
 244 C, $stat_{water}$ is equal to 0.

245 **2.3.2 Carbon stock partitioning method**

246 SEIB-DGVM allocates and stores the biomass carbon in four pools of woody PFT (foliage, trunk, root,
 247 and stock) and three pools of grass PFT (foliage, root, and stock). To investigate the fractional variability
 248 of carbon sequestration potential between the pools, we partitioned potential vegetation carbon stocks
 249 based on the physiological function of the plant (Figure A1). The root-shoot ratio (R/S) has been used to
 250 distinguish and investigate the ratio of below-ground biomass (root biomass) and above-ground biomass
 251 (shoot biomass) (Zhang et al., 2016). In this study, we adjusted the method of calculating the R/S ratio
 252 by distinguishing between the light-gathering vegetation biomass carbon stock (LVBC) and the water-
 253 gathering vegetation biomass carbon stock (WVBC). LVBC represents the biomass carbon invested by
 254 plant is used to gather sunlight, including biomass carbon from woody foliage, woody trunk, and grass
 255 foliage. WVBC represents biomass carbon used to gather water, including biomass carbon from woody
 256 fine roots and grass fine roots, excluding the stock pool. Stock biomass is used for foliation after dormant

257 phase and after fires ~~in~~ PFTs, which is reserve resource in each individual tree. Fine root biomass is just
 258 a tiny fraction to the total biomass, but is has a very high turnover rate and determines the capacity of
 259 vegetation to absorb soil water. Thus,

$$260 \frac{LVBC}{WVBC} = \frac{WT_{mass_{leaf}} + WT_{mass_{trunk}} + G_{mass_{leaf}}}{WT_{mass_{root}} + G_{mass_{root}}} \times 100\% \quad (9)$$

261 where ~~GVBC-LVBC~~ is ~~light-gatheringaboveground~~ vegetation biomass carbon stock (kg C m⁻²); WVBC
 262 is ~~water-gatheringbelowground~~ vegetation biomass carbon stock (kg C m⁻²); ~~WT~~*mass_{leaf}* is the leaf
 263 biomass carbon stock of ~~woody vegetation~~~~wood~~ (kg C m⁻²); and ~~WT~~*mass_{trunk}* is the trunk biomass
 264 carbon stock of ~~wood-tree~~ (kg C m⁻²), including both branch and structural roots. This biomass is
 265 simplistically attributed to ~~light-gathering vegetationaboveground~~ organs and is used primarily to support
 266 the plant. *G_{mass_{leaf}}* is the leaf biomass carbon stock of grass (kg C m⁻²); whereas ~~WT~~*mass_{root}* and
 267 *G_{mass_{root}}* are functional root (fine roots) biomass carbon stocks of ~~wood-tree~~ and grass, separately (kg
 268 C m⁻²), which absorb water and nutrition from soil.

269 2.4 Experimental design

270 2.4.1 Setup of model runs

271 SEIB-DGVM simulations begin with seeds of selected PFTs planted in bare ground. The establishment
 272 of PFTs seeds are determined by the climatic conditions in each grid cell. We inputted the transient
 273 climate data from 1901 to 1915 to spin up the model in a repetitive loop. No obvious trend in climatic
 274 factors was observed during this period (Tei et al., 2017). A spin-up period of 1050 years was necessary
 275 to bring the terrestrial vegetation carbon cycle into a dynamic equilibrium. To reach quasi-equilibrium
 276 in the vegetation biomass, about 1000 years of simulation was required as a spin-up procedure.

277 2.4.2 Factorial simulation scheme

Table 1. List of factorial simulations used in this study

Factorial simulation	CO ₂ concentration	Precipitation	Temperature	Radiation	Other drivers
S1	√	√	√	√	√
S2	√				
S3	√	√			
S4	√		√		
S5	√			√	
S6	√				√

Note: In factorial simulation S1, historical atmospheric CO₂ concentration and historical climate fields from the CRU data set were used. In simulation S2, only historical atmospheric CO₂ concentration was used, and climate variables of the transient period (1901–1915) were repeatedly input. In simulation S3 (or S4, S5), only historical atmospheric CO₂ concentrations and precipitation (or temperature, radiation) were input, and climate variables of the transient period (1901–1915) were repeatedly input. In the last simulation S6, only historical atmospheric CO₂ concentrations and other climate variables were input, including wind velocity and relative humidity.

278 In order to further quantify the relative contributions of varying atmospheric CO₂ concentrations,
279 precipitation, temperature, radiation, and other factors (wind velocity and relative humidity), we
280 performed six factorial simulations. ~~Other factors included wind velocity and relative humidity, which~~
281 ~~had remarkable effects on the change in vegetation carbon stock at zonal scale.~~ In simulation S1,
282 atmospheric CO₂ concentration and all of climate variables were varied. In simulation S2, only
283 atmospheric CO₂ concentration was varied, and climate variables were held constant (Climate variables
284 of the transient period (1901-1915) were repeatedly inputted). In simulation S3 (or S4, S5), atmospheric
285 CO₂ and precipitation (or temperature, radiation) were varied, and other climate variables were held
286 constant. In simulation S6, atmospheric CO₂, wind velocity, and relative humidity were varied, and other
287 climate variables were held constant. Finally, S2 was used to evaluate the effects of CO₂ fertilization on
288 carbon stock variation. The differences of S2-S3, S2-S4, S2-S5, and S2-S6 were used to evaluate the
289 response of carbon stock growth to precipitation, temperature, radiation, and other drivers, respectively.

290 **2.4.3 Non-parametric test methods**

291 Each driving factor (atmosphere CO₂, precipitation, temperature, and radiation) has a different influence
292 on the carbon stock, so it is difficult to make a simple pre-assumption about the population distribution
293 pattern for factorial simulations. We used the non-parametric Mann-Kendall and Sen's slope estimator
294 statistical tests (Gocic and Trajkovic, 2013) to assess the ability of SEIB-DGVM to simulate the response
295 patterns of carbon storage potential to a change in climate and CO₂ concentrations. We regressed the
296 simulated hundred-year mean global average carbon stock time series to reveal the accumulative
297 influences of the single variables based on the factorial simulations where only one or two drivers were
298 varied. As shown in Figures A2, ~~–~~ and A3, detection trends of LVBC and WVBC for all driving factors
299 performed statistically well (in agreement at the 95% confidence intervals), indicating this analytical
300 method was suitable for trend attribution at the global scale.

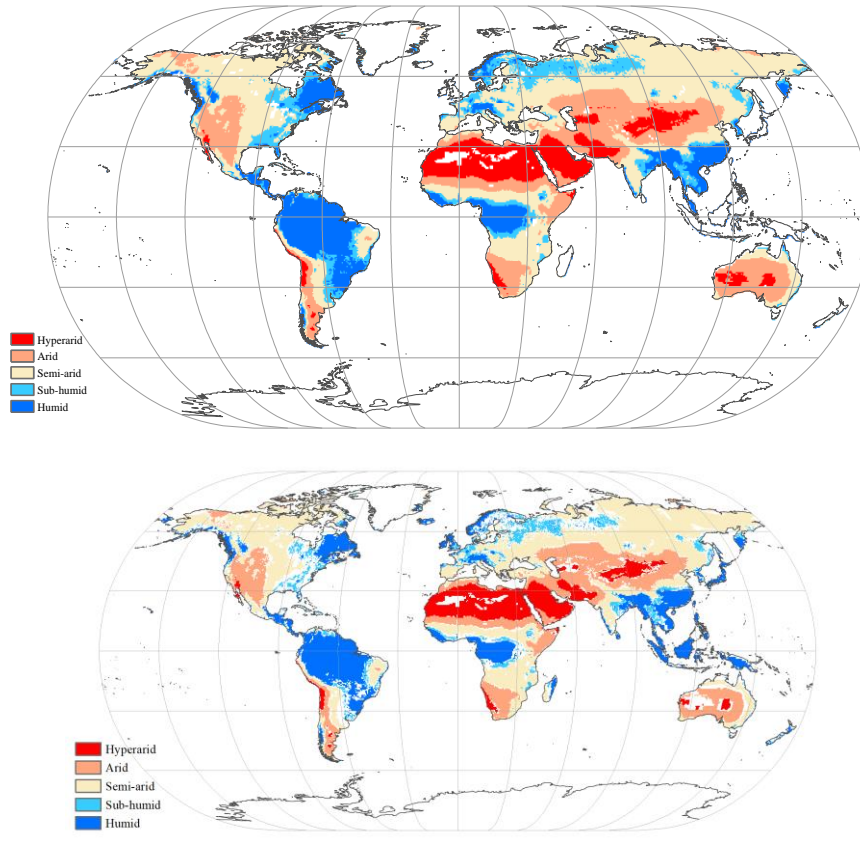


Figure 1. Global spatial patterns of water availability. Spatial variations in water availability were categorized based on ~~the multiyear a 115 year~~ average aridity index (AI), defined as the ratio of the multiyear mean precipitation to the potential evapotranspiration. Categories include: hyper-arid ($AI \leq 0.05$), arid ($0.05 < AI \leq 0.2$), semi-arid ($0.2 < AI \leq 0.5$), sub-humid ($0.5 < AI \leq 0.65$), and humid ($AI > 0.65$).

302 Locally available water strongly regulates and limits the response of carbon stocks to changes in climate
 303 and CO_2 . We used aridity index (AI) to distinguish between the global hydrological regions for
 304 comparing the long-term trend in carbon stocks over different hydrological environments, and for
 305 quantifying the influences of each hydrological environment on the variations in the trends. The AI was
 306 defined as:

$$307 \quad AI = \frac{\bar{P}}{\overline{ET_p}} \quad (10)$$

308 where \bar{P} is the multiyear mean precipitation ($mm \text{ year}^{-1}$); and $\overline{ET_p}$ is the multiyear mean potential
 309 evapotranspiration ($mm \text{ year}^{-1}$), which was calculated by the Penman-Monteith model (Monteith and
 310 Unsworth, 1990). As in a previous study (Chen et al., 2019), five hydrological regions (~~Figure 1~~) were

311 categorized based on a ~~115 year average AI (1901-2015)~~: including a hyper-arid region ($AI \leq 0.05$),
312 arid region ($0.05 < AI \leq 0.2$), semi-arid region ($0.2 < AI \leq 0.5$), sub-humid region ($0.5 < AI \leq 0.65$), and
313 humid region ($AI > 0.65$). Under the influences of climate change, the hydrological condition was
314 changed in some grid cells (Figure A4). For example, the grid classified as sub-humid zone in the period
315 of 1916-1945 was redefined as semi-arid zone in the period of 1986-2015. In this study, grid cells with
316 consistent hydrological condition between the period of 1916-1945 and the period of 1986-2015 were
317 selected and classified (Figure 1).

318 2.5 Observation dataset for model evaluation

319 A global time series of potential vegetation carbon was modelled by the SEIB-DGVM between 1916-
320 2015. In terrestrial vegetation biomes, there is a high correlation between biomass carbon stock density
321 and NPP per unit (Erb et al., 2016; Kindermann et al., 2008) (Figure A1). Thus, we collected NPP
322 observation dataset and used NPP as a proxy of the carbon stock to assess model accuracy. Ecosystem
323 Model-Data Intercomparison (EMDI) builds upon the accomplishments of the original worldwide
324 synthesis of NPP measurements and associated model driver data prepared by Global Primary Production
325 Data Initiative. We obtained the monitoring station data from the EMDI working group, and then
326 compared their data with modelled multiyear average NPP in the period of 1916-1999 (Figure 2).

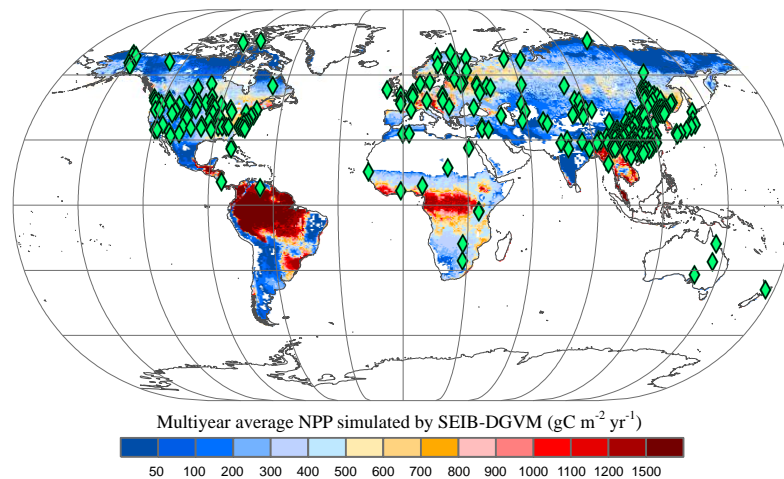


Figure 2. Multiyear average NPP simulated by SEIB-DGVM and EMDI global site distribution. Green rhombuses indicate the monitoring stations of the EMDI.

327 However, *in-situ* observations are sparse for global spatial-temporal validation. Therefore, we used the
328 MOD17A3 products to further verify the simulated potential NPP in the twenty first century. These data
329 were collected by the Moderate Resolution Imaging Spectroradiometer and are some of the most widely

330 used data to assess the accuracy of global model simulations (Gulbeyaz et al., 2018). The natural
331 vegetation zones refer to the hypothetical condition that would prevail in an assumed absence of
332 anthropogenic activity, but under historical climate fields (Erb et al., 2018; Haberl et al., 2014). The
333 potential NPP is defined as that assimilated carbon stored in natural vegetation without the disturbance
334 of anthropogenic activities (Erb et al., 2018).

335

336 In order to distinguish the distribution of vegetation zones without anthropogenic disturbance, we
337 obtained global land cover types in the period 2001-2015 from MCD12C1 (Table A1). ~~It was~~We defined
338 ~~as~~-vegetation grid cells as those whose largest component was that the land cover type of this grid is
339 evergreen needleleaf forest, evergreen broadleaf forest, deciduous needleleaf forest, ~~deciduous~~
340 broadleaf forest, mixed forest, closed shrublands, open shrublands, woody savannas, savannas or
341 grasslands. ~~Grid covered by other 7 land types was defined as non-vegetation grid. Then, we calculated~~
342 ~~the proportion of each land cover types in corresponding 0.5° grid unit. The land cover type of grid unit~~
343 ~~was determined by the max proportion among 17 land cover types.—~~ Other grid cells were excluded from
344 our analysis.

345

346 Part of grids covered by grassland were grazed by livestock, leading to the decrease of NPP of grass
347 PFTs. We obtained land-use forcing data from Land-Use Harmonization (LUH2) to map the distribution
348 of managed pasture data from 2001 to 2015 (Hurt et al., 2020). As shown in Figure ~~A4~~A5, grassland in
349 eastern Asia, western Europe, south central Africa, and western South America were severely affected
350 by grazing. ~~To~~For exhibit the disturbance of managed pasture, we calculated the mean fraction of
351 managed pasture within the corresponding 0.5° grid unit. When the fraction of managed pasture over
352 ~~10%~~0.01, the grid ~~covered by grassland~~ was considered to be affected by managed pasture. To reduce
353 the interference effects of livestock grazing, we first removed the grids affected by managed pasture.
354 Then, we map the distribution of natural vegetation zones without anthropogenic disturbance (Figure
355 A6). We declare that this exclusion method is only used for potential NPP comparison.~~We filtered~~
356 ~~grassland affected by pasture to map the distribution of natural vegetation zones without anthropogenic~~
357 ~~disturbance (Figure A5).~~

358 **3 Results and discussion**

359 **3.1 Evaluation of SEIB-DGVM**

360 Figure 3 illustrates the comparison between model simulated and observed multi-year mean NPP during
361 1916-1999. The determined coefficient (R^2) between EMDI observed and estimated multiyear average
362 NPP of 669 *in-situ* observations is 0.54, which is significant at the $p=0.01$ level. The slope of the
363 regressed line is 0.70 during the twentieth century.

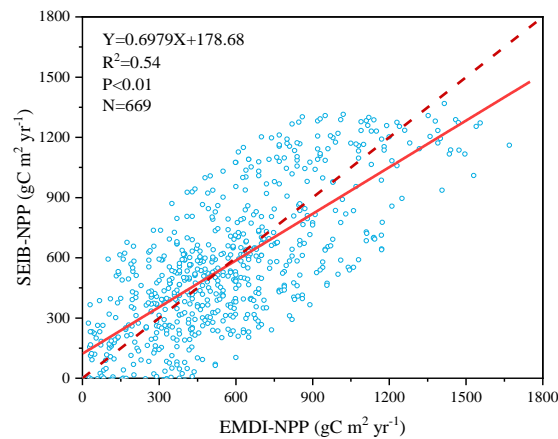


Figure 3. Comparison of multiyear average NPP calculated by SEIB-DGVM and EMDI for the twentieth century. The solid line is the best fit curve; and the dashed line represents a perfect correspondence in the results of the two.

364 Based on land cover types dataset from 2001 to 2015, we obtained NPP-MOD17A3 data in natural
365 vegetation zones without anthropogenic disturbance at the same period. Figure 4 shows that the modelled
366 NPP from the SEIB-DGVM exhibited a high degree of consistency with the NPP-MOD17A3 data in
367 natural vegetation zones over the period ($R^2=0.63$, $p<0.05$). The general spatiotemporal agreement
368 between the simulated NPP derived from SEIB-DGVM with *in-situ* observations and derived from
369 satellites reveals that it is reasonable to use the SEIB-DGVM simulations to evaluate the same
370 mechanisms controlling global potential biomass carbon stocks of vegetation.

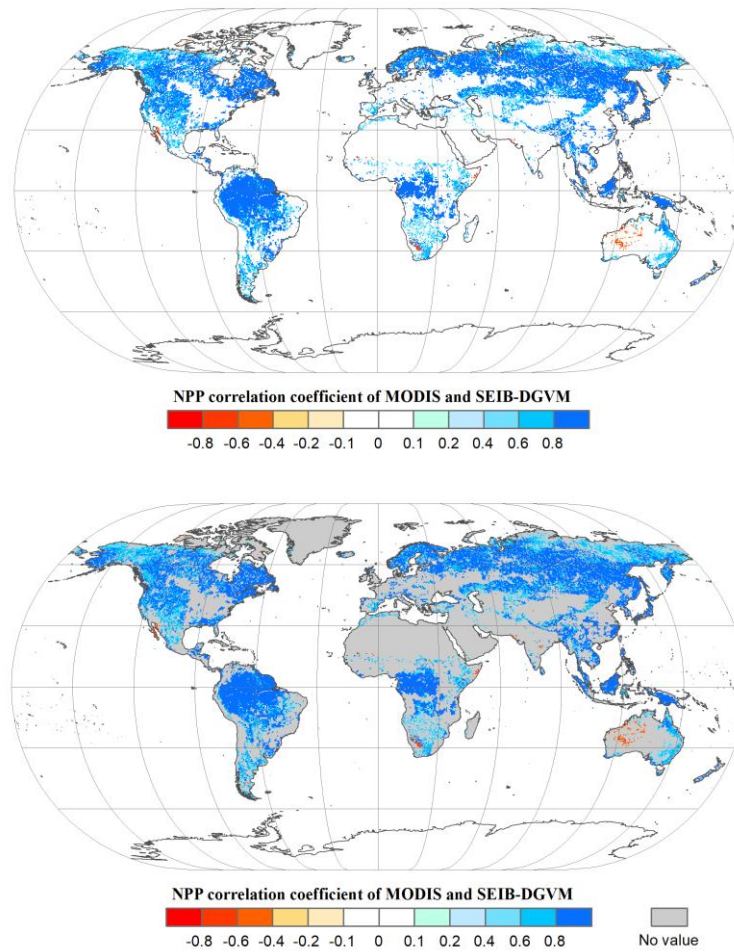


Figure 4. Spatial patterns in the potential NPP correlation coefficients ($P < 0.05$) between SEIB-DGVM and MODIS between 2001–2015. These data were used to validate SEIB-DGVM.

371 Finally, the modelled result of potential vegetation biomass carbon stock was compared with current
 372 existing data from the literature and state-of-the-art datasets. Figure 5 shows that the modelled results are
 373 within the range of potential carbon stocks, which indicate that the SEIB-DGVM reliably simulated the
 374 carbon stock dynamics.

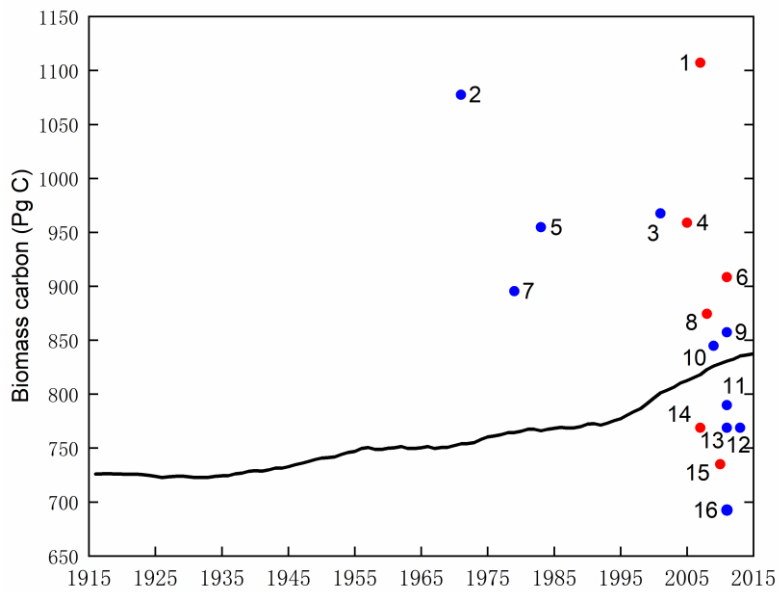
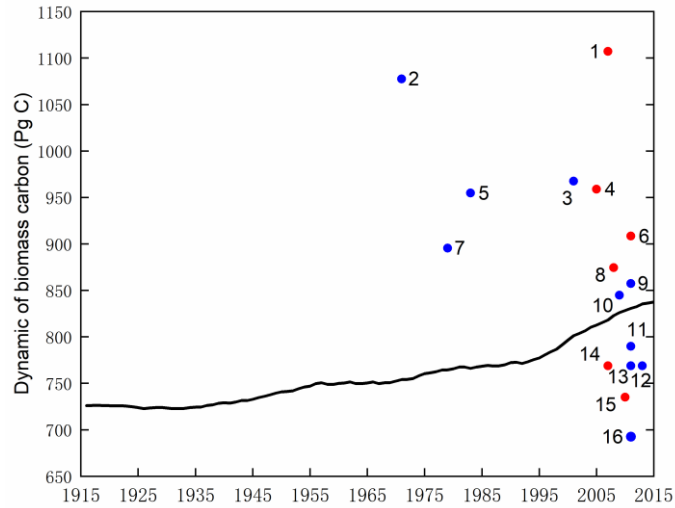
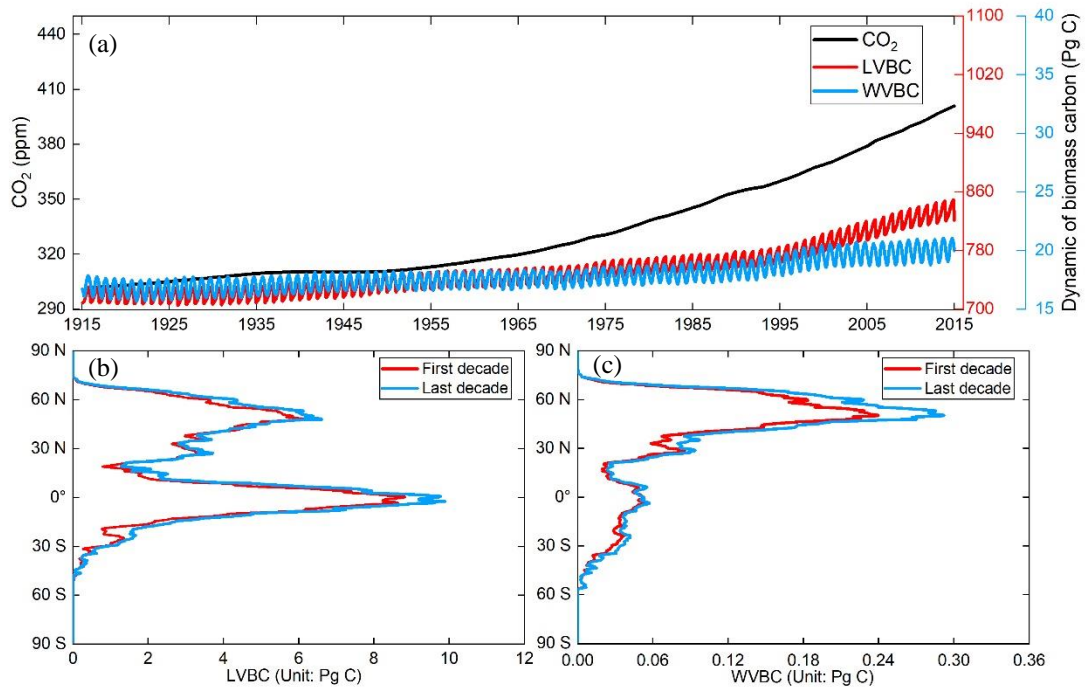


Figure 5. Estimates of the potential vegetation biomass carbon stock from the literature (blue plot), state-of-the-art datasets (red plot) and this study (black line). Datasets are from the following studies: (1)(Erb et al., 2018; Erb et al., 2007), (2)(Bazilevich et al., 1971), (3)(Saugier et al., 2001), (4)(Erb et al., 2018; Bartholome and Belward, 2005), (5)(Olson et al., 1983), (6)(Erb et al., 2018; Pan et al., 2011), (7)(Ajtay et al., 1979), (8)Erb et al., 2018; Ruesch and Gibbs, 2008), (9)(Kaplan et al., 2011), (10)(Shevliakova et al., 2009), (11)(Kaplan et al., 2011), (12)(Pan et al., 2013), (13)(Prentice et al., 2011), (14)(Erb et al., 2018; Erb et al., 2007), (15)(Erb et al., 2018; West et al., 2010), (16)(Hurt et al., 2011).–

375 **3.2 Enhanced carbon stocks and its fractions**

376 We distinguished the changes of LVBC and WVBC from total vegetation carbon stocks. The historical

377 temporal trends over the period are ~~shown~~ showed in Figure 6a. The potential vegetation carbon stock
 378 exhibits a net increase of 119.26 ± 2.44 Pg C in the last century (± 2.44 represents intra-annual fluctuation
 379 in carbon stock, which is the difference between maximum value and a minimum value of carbon stock
 380 within the year). Based on Pearson correlation analysis, this increasing trend of annual average carbon
 381 stock exhibits a robust agreement with the dramatic increase in atmospheric CO₂ concentration
 382 ($R^2=0.9677$, $p<0.001$), suggesting that the carbon stock is strongly affected by CO₂ fertilization.
 383 Meanwhile, the positive correlation between the carbon stock and CO₂ generally extends across LVBC
 384 ($R^2=0.9669$) and WVBC ($R^2=0.9622$). After the value of the global terrestrial carbon stock and trends
 385 were partitioned among the vegetation functional classes, we see that LVBC increases 116.18 ± 2.34 Pg
 386 C (or $\sim 15.60\%$), which explains 97.42% of total carbon stock increasing trend and dominates the positive
 387 global carbon stock trend; WVBC also increases 3.08 ± 0.14 Pg C (or $\sim 18.03\%$) over the past century.



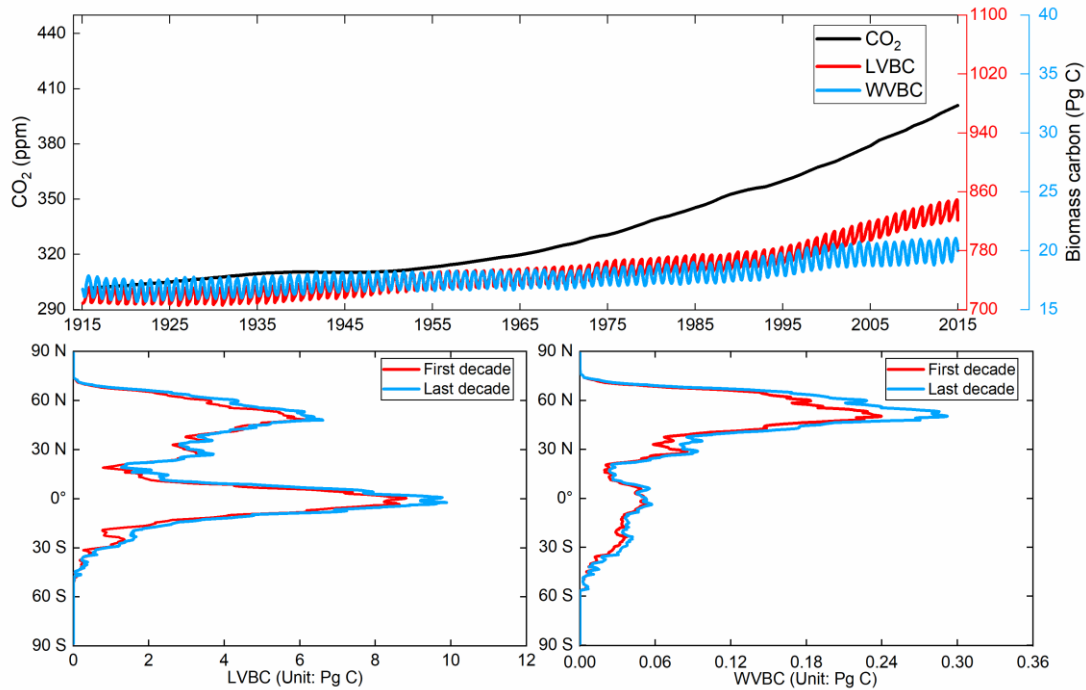


Figure 6. Global potential biomass carbon stocks of vegetation during the past 100 years. (a) The evolution of global potential biomass stocks (LVBC+WVBC), along with changes in biomass stocks that can be attributed to the variability and trend of LVBC and WVBC through the twentieth century. The red line represents the monthly value of LVBC, the blue line represents the monthly value of WVBC, and the black line represents the annual value of CO₂ concentration. **(b, c)** Zonal averaged sums of the annual LVBC and WVBC for latitudinal bands during the first decade (1916–1925, red line) and the last decade (2006–2015, blue line) shows the increased carbon stock capacity.

388 The global distributions of the decadal-average change in LVBC and WVBC are shown in Figures 6b
 389 and 6c, respectively. The significant historical changes in climate and CO₂ enhance the carbon stock of
 390 the terrestrial ecosystem, and their positive influences are broadly distributed across a latitudinal north–
 391 south gradient. The latitudinal bands of increasing annual LVBC are mainly distributed in the tropical
 392 and boreal latitudes, which is consistent with Figure 7b. The decadal and inter-annual variabilities of
 393 LVBC are dominated by the tropical and semi-arid zones where large portions of the zones are highly
 394 productive (Ahlstrom et al., 2015; Poulter et al., 2014). Tropical LVBC dominates the long-term trend
 395 of global LVBC in the last hundred years. Compared with LVBC, the increase of tropical WVBC is light.
 396 There is a single peak in the spatial variation of annual WVBC (Figure 6c and Figure 7c).
 397 WVBC exhibits robust growth at most latitudes, and increases mainly in boreal latitudes.

398 **3.3 Spatial variability in estimated LVBC and WVBC trends**

399 In Figures 7(a) and 7(b), total carbon stock and LVBC exhibited a significantly increasing trend in eastern
400 South America, southern Africa, and northern Asia, while they declined in central North America,
401 northwest South America, and central Africa. WVBC showed a more widely increasing tendency in
402 North America, southeastern South America, and Europe, while had a ~~decrease-decreasing~~ trend in part
403 zones of Asian. We find that the total carbon stock as well as the light- and water-gathering vegetation
404 biomass carbon stocks over the period of 1916–2015 exhibited a remarkable spatial heterogeneity. Figure
405 7a shows that an increase in vegetation carbon stocks occurred over zones and global aggregate levels
406 during the entire study period. About 57.39% of the terrestrial grids exhibited an increase with a
407 noticeable trend ($p < 0.05$) in biomass carbon stock; 53.82% of global grids possessed increases that were
408 statistically significant at the $p = 0.01$ level. To determine the contributions of each fraction (LVBC,
409 WVBC) to the total change in the potential vegetation carbon stock, we partitioned and present the
410 historical spatial and temporal patterns for each fraction separately (Figure 7b, 7c). LVBC contributes
411 97.33% to the incremental change of total carbon stock (116.18 ± 2.34 Pg C), with about 51.32% of the
412 grids possessing a noticeable positive trend ($p = 0.01$). Generally, spatial patterns of LVBC and the total
413 carbon stock are consistent (Figure 7a, 7b), which further supports the argument that LVBC dominates
414 the trend in carbon stocks in most zones. Although the proportion of the total change in carbon stocks is
415 small (2.58% of total carbon stock increase), about 61.00% of the land surface shows an increase in
416 WVBC; of these terrestrial grids, 55.81% was characterized by a significant $p = 0.01$ increase.

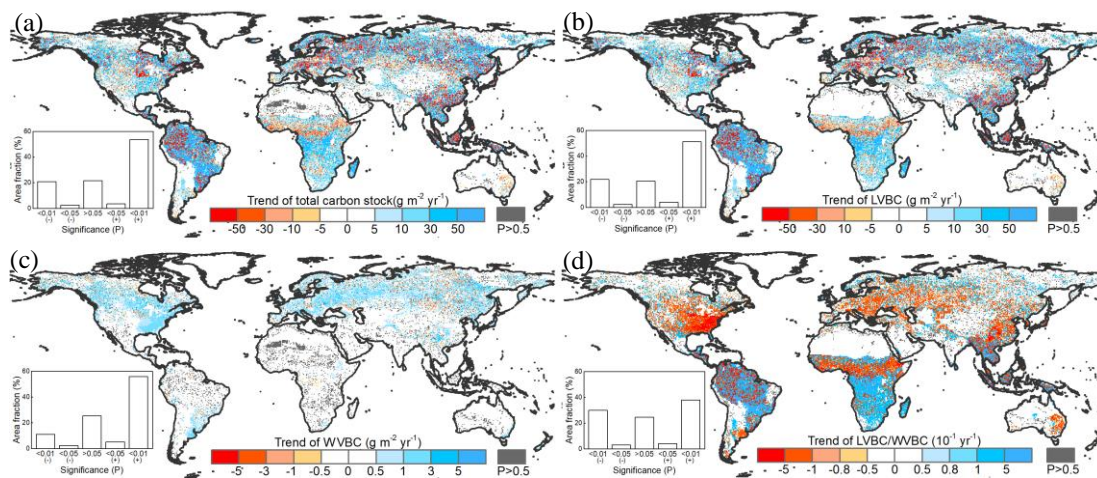


Figure 7. Spatial patterns in the trends of potential vegetation carbon stocks and their fractions

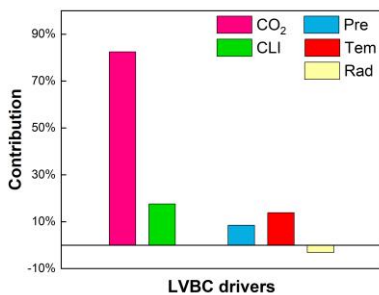
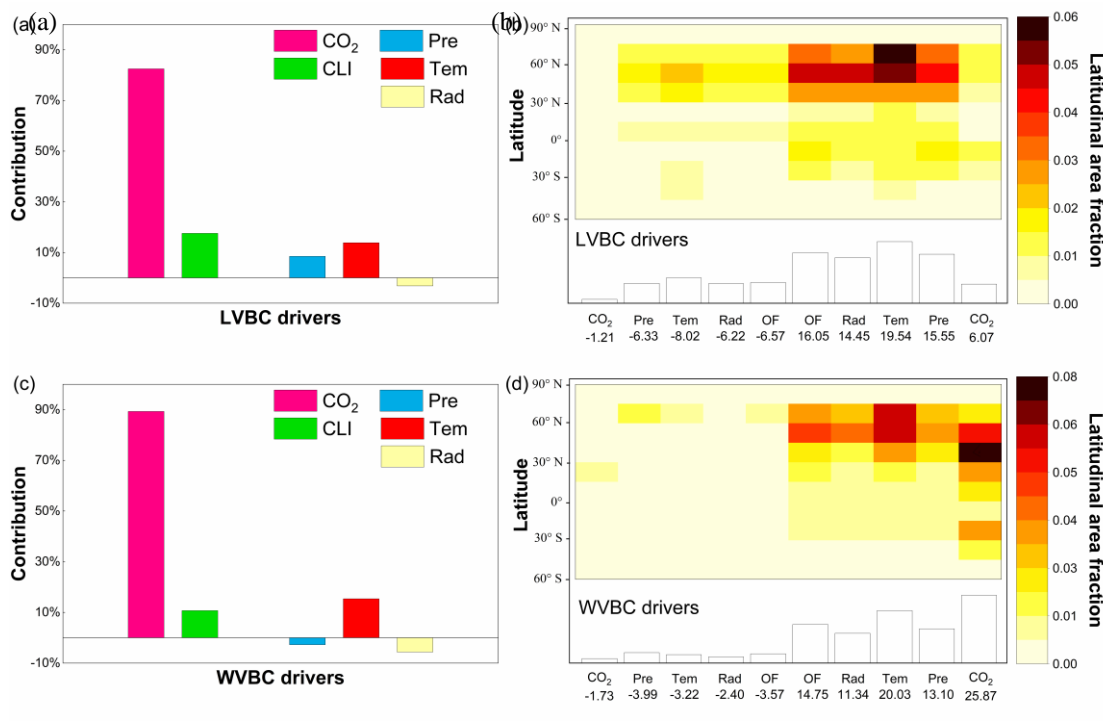
from 1916 to 2015. Difference induced by changes in climate and CO₂ in terrestrial biomass carbon stock (a), LVBC (b), and WVBC (c) during the historic period 1916–2015. The blue bar indicates the significantly increasing trends and the red bar indicates the significantly decreasing trends in carbon stocks. (d) Trend in the LVBC/WVBC ratio from 1916 to 2015. The blue bar indicates significantly increasing trends in the ratio, and vice versa. The grey bar indicates the trend is statistically insignificant ($P > 0.05$). The sub-graphs show the significant test results. A ‘+’ symbol indicates a positive trend, and vice versa.

417 Under the influences of a changing climate and CO₂ concentrations, there is a slight increase in the ratio
418 of global LVBC/WVBC; the rate of increase is 0.0171 yr⁻¹ in the last hundred years, which is significant
419 at the 0.01 level (Figure 7d). About 42.08% of the terrestrial grids exhibited an increase with a noticeable
420 trend ($p < 0.05$) in the ratio of LVBC and WVBC; 37.95% of global grids possessed increases that were
421 statistically significant at the $p = 0.01$ level. Meanwhile, 33.32% of the land surface shows a significant
422 decrease in LVBC/WVBC; of these terrestrial grids, 30.06% was characterized by a significant $p = 0.01$
423 decrease. Zones with noticeable increases in the ratio of LVBC to WVBC are mainly located in southern
424 Africa, central South America, and northern Eurasia. Negative trends in LVBC/WVBC ratios are found
425 in northern America, southern Europe, and tropical Africa.

426 3.4 Responses of LVBC and WVBC to environmental drivers

427 The responses of LVBC and WVBC to changes in climate and CO₂ are both positive at the global level
428 (Figure 8a, 8c), although zonally, they exhibit both negative and positive responses (Figure 8b, 8d).
429 Based on the results of factorial simulations and Mann-Kendall+Sen tests, CO₂ fertilization explains the
430 largest proportion of the change in the carbon stock; about 82.45% change in LVBC was positive (Figure
431 8a), whereas 89.28% of the change in WVBC was positive (Figure 8c). In factorial simulation S2, the
432 long-term trend of LVBC was 15.521 g C m⁻² yr⁻¹ and that of WVBC was 0.435 g C m⁻² yr⁻¹ at the
433 period from 1916 to 2015 (Figure A2a and Figure A3a). The separately simulated LVBC and WVBC
434 increased by 80.98 Pg C and 2.66 Pg C with increasing atmospheric CO₂ concentrations (from 301.73
435 ppm in 1916 to 400.83 ppm in 2015). The other climatic drivers (precipitation, temperature, radiation,
436 humidity, and wind speed) remained at baseline values. While the increase or decrease in the carbon
437 stock may be attributed to more than one driving factor, within any specified grid, the one with the highest

438 positive or negative contribution is the dominated driver that consistently resulted in the highest increase
 439 or decrease in the carbon stock for that grid. While the increase or decrease in the carbon stock may be
 440 attributed to more than one driving factor, within any specified grid, the one with the highest contribution
 441 was the driver that consistently resulted in the highest increase or decrease in the carbon stock for that
 442 grid. The spatial pattern illustrates that CO₂ dominates the variability in LVBC in 7.28% of the zones,
 443 including 1.21% of the zones that exhibited a negative change and 6.07% that exhibited a positive change
 444 (Figure 8b). CO₂ dominates the variability in WVBC in 27.60% of the zones, including 1.73% of the
 445 zones that exhibited a negative change and 25.87% of zones with a positive change (Figure 8d). Under
 446 the effect of CO₂ fertilization, grids with increased trend in WVBC mainly distribute in boreal latitudes
 447 (Figure 6c). These trends are consistent with and previous studies (Tharammal et al., 2019; Zhu et al.,
 448 2016; Keenan et al., 2017) in which positive trends occurred, especially for WVBC.



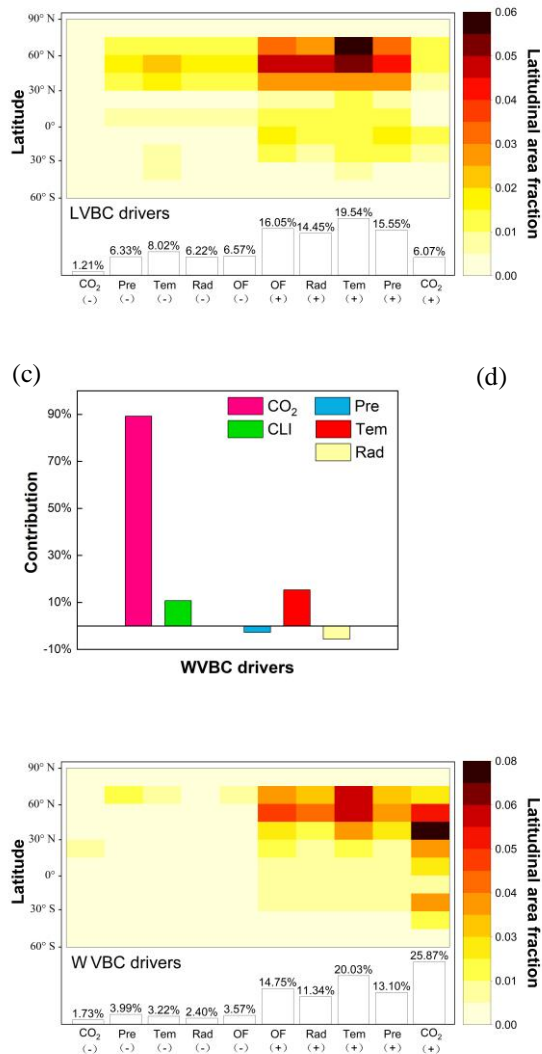
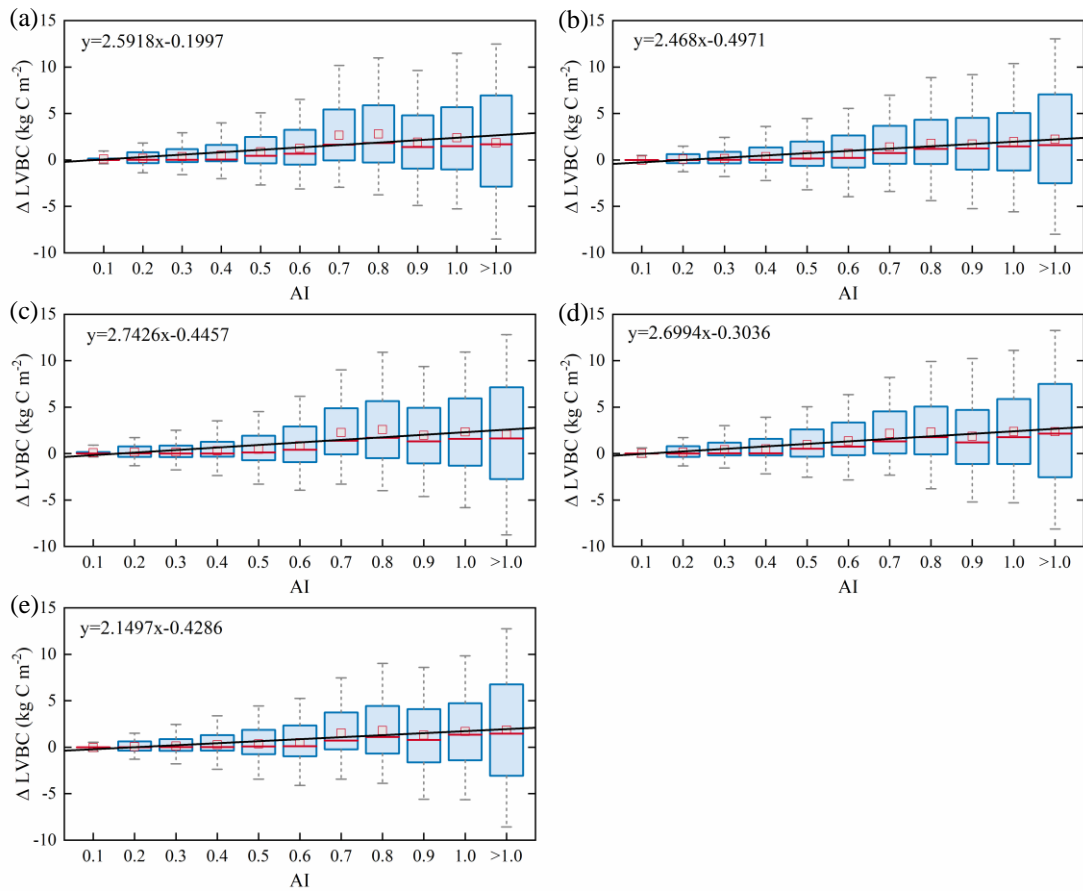


Figure 8. The proportion of change in the vegetation biomass carbon stocks attributed to driving factors. Ratios of the driving factors of CO₂ fertilization effects (CO₂), climate change effects (CLI), precipitation (Pre), temperature (Tem), radiation (Rad) for LVBC (a) and WVBC (c) under the five scenarios using the Mann-Kendall and Sen's slope estimator statistical tests. Attribution of LVBC (b) and WVBC (d) dynamics to driving factors calculated as averages along 15° latitude bands. At local scales, the driving factors include CO₂, Pre, Tem, Rad, and other climate factors (OF). The fraction of global area (%) that is predominantly influenced by the driving factors is showed at the bottom of the bar. A-The '+-' symbol before fraction indicates a positive-negative effect of the driving factor on carbon stock, and vice versa. ~~The fraction of global area (%) that is predominantly influenced by the driving factors is shown at the top of the bar.~~

449 Climate change induced by the greenhouse effect explains part of the increase in carbon stocks, but unlike

450 CO₂ fertilization, climate has dramatic negative effects on some vegetated zones. Figure 8a illustrates
451 that temperature is the largest climatic contributor to the change in LVBC (13.83%, 2.572 g m⁻² yr⁻¹),
452 followed by precipitation (8.51%, 1.572 g m⁻² yr⁻¹) and radiation (-3.19%, -0.649 g m⁻² yr⁻¹). The spatial
453 distribution shows that temperature predominantly influences the change in LVBC (Figure 8b),
454 influencing over 27.56% of the global vegetated zones, followed by precipitation (21.88%) and radiation
455 (20.67%). Figure 8c shows there ~~is~~ are ~~difference in the~~ negative effects and contributions of
456 precipitation ~~to~~ on the change in WVBC at the global level (-2.76%, -0.013 g m⁻² yr⁻¹). Temperature is
457 the largest climatic contributor to the change in WVBC (15.36%, 0.075 g m⁻² yr⁻¹), followed by radiation
458 (-5.63%, -0.027 g m⁻² yr⁻¹). Modelled WVBC trends based on the factorial simulations have similar
459 spatiotemporal patterns to LVBC (Figures A2 and A3), the spatial patterns of light- and water-gathering
460 carbon stocks show a significantly increasing trend in the most of boreal zones. In the Southern
461 Hemisphere, the trends of WVBC are extensively statistically insignificant in all factorial simulations,
462 and only a small proportion of grids show a significantly increasing trend. There is a significantly
463 increasing trend in LVBC in south-central Africa and northern South America. The effects of temperature
464 on WVBC are stronger than LVBC, because temperature has a stronger effect on the metabolism process
465 of root growth, dominating the turnover rate and the costs of maintenance respiration in root growth
466 process (Gill and Jackson, 2000). It should be noted that trends in the global carbon stock can be largely
467 attributed to the influences of CO₂, precipitation, temperature, and radiation (Figure 8). Nonetheless, at
468 the zonal scale, the contributions of other factors should be considered, such as humidity and wind speed.
469 The effects of these other factors dominate trends in LVBC in over 16.05% of the zones that increased
470 and 6.57% of the zones that decreased. In the case of changes in WVBC, other factors were dominant
471 drivers in over 14.75% of the zones that increased and 3.57% of zones that decreased. Under the effect
472 of climate, the variability of LVBC and WVBC is positive in most zones, promoting the noticeable
473 increase of carbon stocks in boreal latitudes.

3.5 Constraints imposed by water limitations



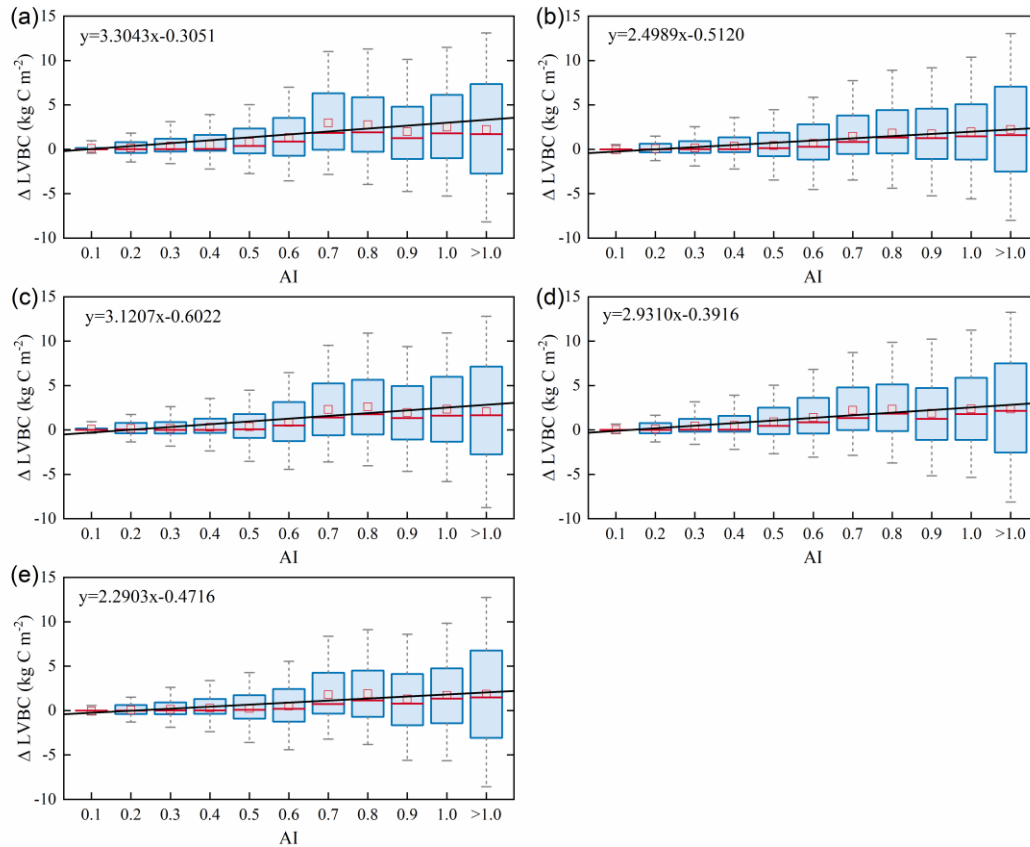
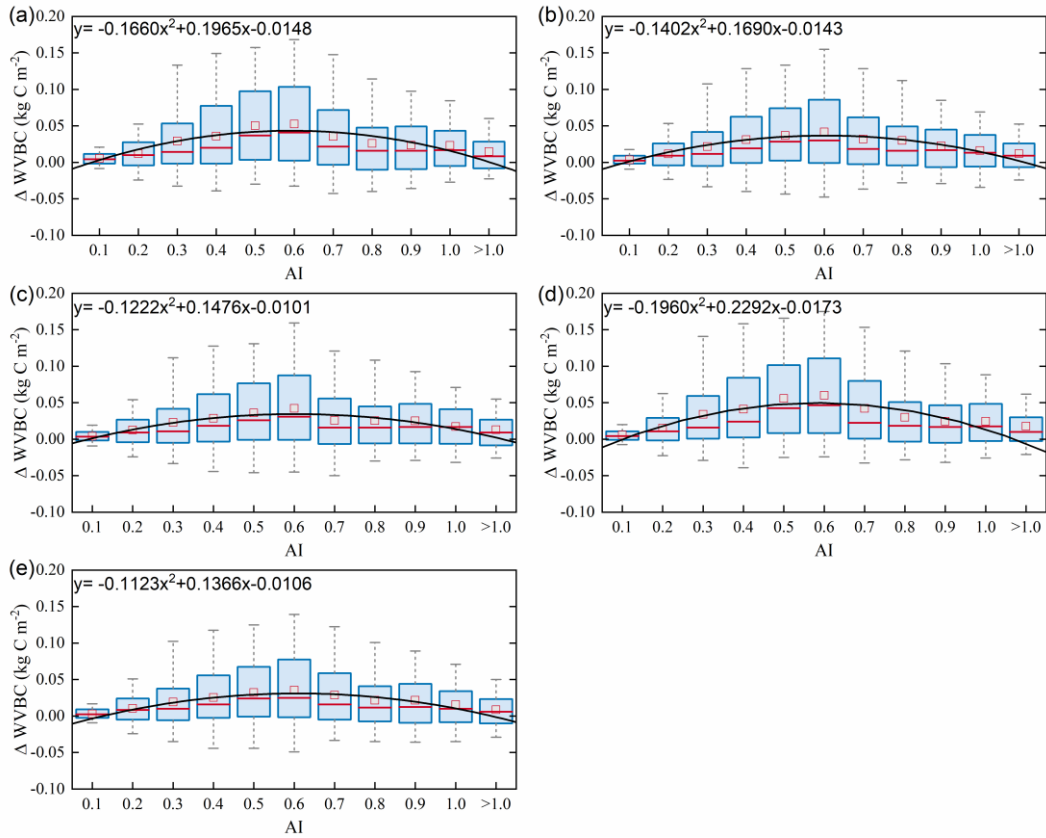


Figure 9. Relationships in the incremental change between AI and LVBC over the hydrological zones grid cells (Figure 1). Magnitude of change in LVBC in the historical scenario S1 (a), CO₂ in scenario S2 (b), CO₂ + precipitation in scenario S3 (c), CO₂ + temperature in scenario S4 (d), and CO₂ + radiation in scenario S5 (e). Range of the box is 25%-75% of values; range of the whiskers is 10%-90% of values; the small red square is average value; the red line is the median line; and the black line is the fitted curve. Positive value of the Y axis represents the magnitude of increased LVBC from 1916 to 2015 under water-limitations conditions, and vice versa. AI of grid cells is calculated by multiyear average precipitation and multiyear average potential evapotranspiration in the period of 1916-2015. Categories of hydrological zones include: hyper-arid ($AI \leq 0.05$), arid ($0.05 < AI \leq 0.2$), semi-arid ($0.2 < AI \leq 0.5$), sub-humid ($0.5 < AI \leq 0.65$), and humid ($AI > 0.65$).

475 Terrestrial water availability emerged as a key regulator of terrestrial carbon storage, by affecting the
 476 response mechanism of the vegetation carbon stock to changes in driving factors. As shown in Figures 9
 477 and 10, with then accumulated increase change of LVBC and WVBC in the period of 1916 to 2015 in
 478 across the aridity index (i.e., an increase in available water), the magnitude and range in variations
 479 responses of LVBC density and WVBC density gradually enhance increase. Based on the results of

480 ~~historical simulation (Figure 9) factorial simulations~~, we find a positive relationship between LVBC and
481 ~~water pressure aridity index~~. In extreme water stress, the increase of LVBC tends to zero and plants stop
482 ~~increasing their carbon storage growing~~. There is no obvious ~~different-difference~~ in the slopes of fitting
483 curves between factorial simulations, ~~which shows the robustness in the response of LVBC to the change~~
484 ~~of water stress~~. The pattern of the enhanced magnitude and range of variation in the WVBC density is
485 unimodal with water stress gradient in all factorial simulations. With the increasing of AI, the magnitude
486 of change in WVBC increases at first and then decreases finally. The mitigation of water stress promotes
487 WVBC increase, while excess surface water limits the response of WVBC to changes in climate and
488 CO₂. These results reveal that the carbon stock increases stimulated by changes in climate and CO₂ are
489 constrained by water available. With increased warming, water limitations are expected to increasingly
490 limit the carbon stock increase, specially at arid regions. To further reveal the controls of water limitation
491 on the responses of inner carbon storages to each driver, we analyse the long-term variability of potential
492 vegetation carbon stocks by means of factorial simulations for each hydrological region (Figure 1).
493 ~~Figure A7b shows that the maximum change magnitude of LVBC density across all factorial simulation~~
494 ~~is 1.202 kg C m⁻² in the hyper-arid regions for the 1916-2015 period. As shown in Figure A7f, the~~
495 ~~maximum change magnitude of LVBC density in humid regions is 6.068 kg C m⁻² during the same~~
496 ~~period. In Figure A8b, the maximum change magnitude of WVBC density across all factorial simulation~~
497 ~~is 0.011 kg C m⁻² in the hyper-arid regions during the time of 1916-2015. In Figure A8f, the maximum~~
498 ~~change magnitude of WVBC density is 0.046 kg C m⁻² in humid regions during the same period.~~
499 ~~Compared with plants lived in aridity regions, plants in humid regions show more dramatic responses to~~
500 ~~the stimulation from drivers' change. With a lessening of water stress (from hyper-arid to humid region),~~
501 ~~the response magnitudes of the carbon stock to the changes of climate and CO₂ gradually become more~~
502 ~~noticeable. The robust pattern in the zonal average density of the carbon stock shows that terrestrial water~~
503 ~~limitations strongly regulate the enhanced magnitude of the carbon stock. It is revealed from Figure A6~~
504 ~~that the increased LVBC density induced by drivers changed from 0.878 ± 0.131 kg C m⁻² in the hyper-~~
505 ~~arid regions to 5.459 ± 0.610 kg C m⁻² in the humid regions during the past hundred years. At global~~
506 ~~scale, the annual mean value of LVBC simulated by each factorial simulation is close. In hyper-arid and~~
507 ~~arid regions, the interannual change of LVBC in historical scenario matches most closely with that of S3~~
508 ~~scenario which considers CO₂ and precipitation effects. Increased WVBC density induced by drivers~~

509 changed from $0.011 \pm 0.001 \text{ kg C m}^{-2}$ in the hyper-arid regions to $0.044 \pm 0.005 \text{ kg C m}^{-2}$ in the humid
510 regions during the same period (Figure A7). The long-term trends of WVBC simulated by each scenario
511 are consistent across different hydrological regions. With a lessening of water stress (from hyper-arid to
512 humid region), the response of the carbon stock to changes in climate and CO_2 gradually became more
513 noticeable. The robust pattern in the zonal average density of the carbon stock shows that terrestrial water
514 limitations strongly limit the enhanced magnitude of the carbon stock.



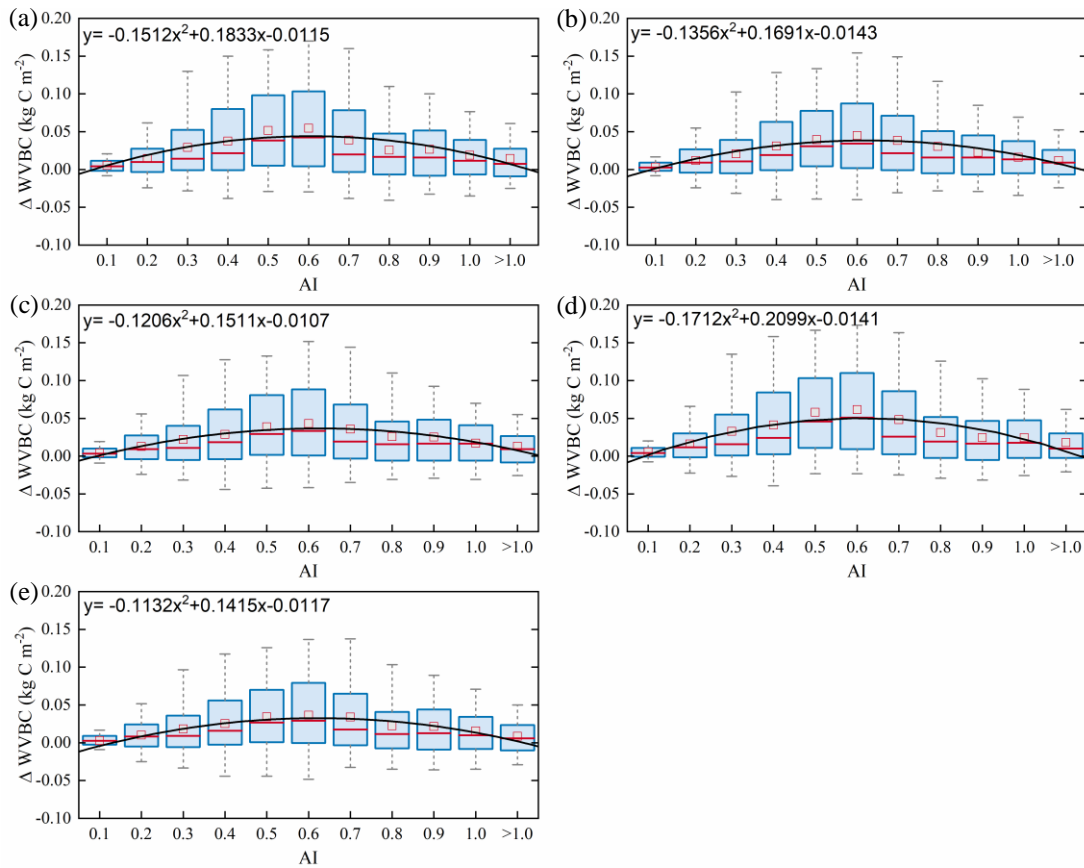


Figure 10. Relationships in the incremental change in AI and WVBC over the hydrological grid cells (Figure 1)the hydrological regions. Magnitude of change in WVBC Modelled WVBC enhanced magnitude in in the historical scenario S1 (a), CO₂ in scenario S2 (b), CO₂ + precipitation in scenario S3 (c), CO₂ + temperature in scenario S4 (d), and CO₂ + radiation in scenario S5 (e). Range of the box is 25%-75% of values; range of the whiskers is 10%-90% of values; the small red square is average value; the red line is the median line, and the black line is the fitted curve. Positive value of the Y axis represents the magnitude of increased WVBC from 1916 to 2015 under water-limitations conditions, and vice ~~versa~~versa. AI of grid cells is calculated by multiyear average precipitation and multiyear average potential evapotranspiration in the period of 1916-2015. Categories of hydrological zones include: hyper-arid (AI ≤ 0.05), arid (0.05 < AI ≤ 0.2), semi-arid (0.2 < AI ≤ 0.5), sub-humid (0.5 < AI ≤ 0.65), and humid (AI > 0.65).

515 Water limitations not only directly reduced the magnitude of the response in the two fractions' carbon
 516 stock (LVBC and WVBC) to changes in climate and CO₂, but also indirectly confined the response
 517 direction of each fractions' carbon stock by transforming vegetation structure and function. Figure 11
 518 illustrates temporal variations in the carbon stock ratio within and between hydrological regions. From

519 hyper-arid zones to humid zones, the fluctuation range (the difference between maximum value and
520 minimum value in each factorial simulation) of LVBC/WVBC ratio significantly changes. The
521 fluctuation magnitudes of LVBC/WVBC in humid and hyper-arid zones are greater than that in other
522 hydrological zones. Compared with plants in hyper-arid zones, plants in humid zones exhibit more
523 significant responses to changes in climate and CO₂. From hyper arid region to humid region, the
524 variation range of ratio between LVBC and WVBC significantly increases. Plants store more assimilated
525 carbon in shoots and leaves in humid regions. Meanwhile, the long-term effects of driver changes have
526 a remarkable influence on this carbon allocation pattern at global level (Figure 7d)The long term effects
527 of driver changes have a positive influence on this carbon allocate pattern. Under the synergistic effect
528 of drivers and water stress, the trends of light- and water-gathering vegetation carbon stock are upward
529 in the past hundred years (Figure 6). However, there is a difference in the increasing rate between LVBC
530 and WVBC, resulting in a dramatic and complicated fluctuation in global LVBC/WVBC ratio (Figure
531 11a). The density of LVBC decreases and that of WVBC increases in hyper-arid and arid zones for all
532 factorial simulations (Figures A7 and A8). So, the ratio of LVBC and WVBC shows a downward trend
533 in these zones. LVBC in semi-arid regions shows upward tendency in the past years (Figure A7d) because
534 of the aridity mitigation. There is an upward trend in WVBC in semi-arid (Figure A8d). Plants in semi-
535 arid still utilize a tolerance strategy and allocates more non-structural carbon to water-gathering
536 vegetation organ to resist water stress, resulting in the decline of LVBC/WVBC ratio. In humid zones,
537 light- and water-gathering biomass carbon stocks both increased in all factorial simulations (Figures A7
538 and A8). The proportion of LVBC increases more than that of WVBC for capturing more resources like
539 CO₂ and radiation energy, leading to an increase in the LVBC/WVBC ratio. The value of LVBC/WVBC
540 in S3 is higher than that in S4 and S5, which represents that precipitation makes more contributions to
541 the change of LVBC/WVBC ratio among meteorological factors. Under the synergistic effect of drivers
542 and water stress, vegetation carbon stock increases, and there is a larger proportion of biomass allocated
543 to, and stored in, light gathering vegetation organs. In drylands (AI≤0.5) of all factorial simulations,
544 light and water gathering biomass carbon stocks both increased but the rate of change in the
545 LVBC/WVBC ratio gradually decreased. To mitigate water stress, plants allocate more assimilated
546 carbon to root for gathering water. In humid zones (AI>0.65), the proportion of LVBC increases more
547 than that of WVBC to obtain more resources like CO₂ and radiation energy, leading to an increase in the

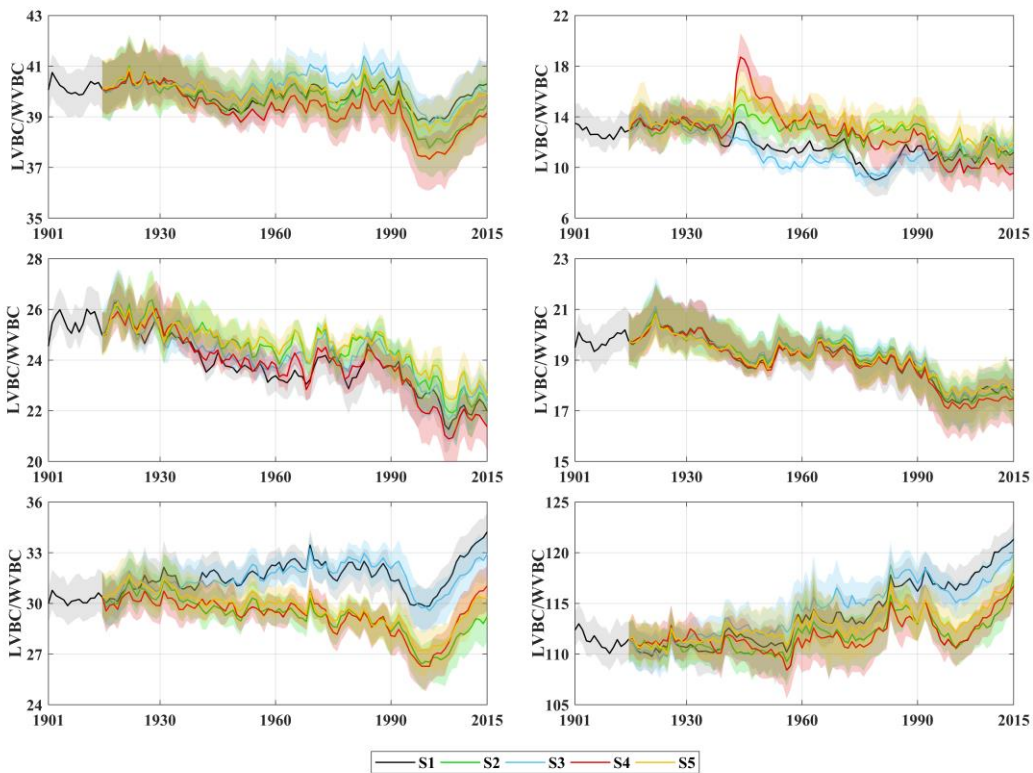
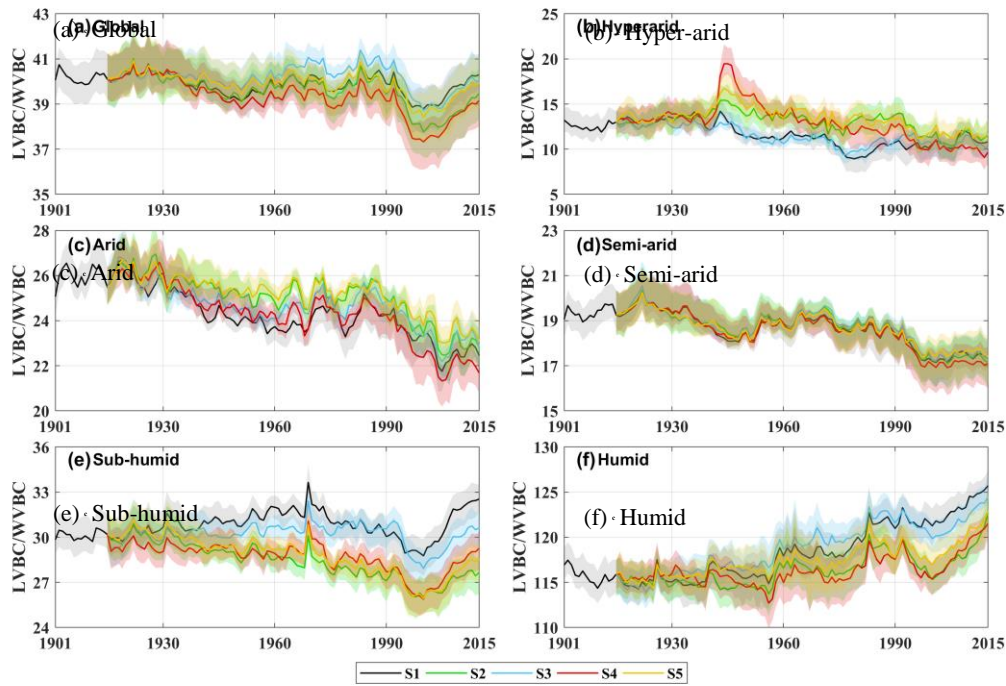


Figure 11. Temporal fluctuations in carbon stock dynamics in vegetation biomass in different factorial simulations. Black indicates historical factorial simulation from 1901-2015, green indicates the CO₂-driven factorial simulation, blue indicates the precipitation-driven factorial simulation, red

indicates the temperature-driving factorial simulation and yellow indicates radiation driven factorial simulation. Uncertainty bounds are provided as shaded areas reflect the intra-annual fluctuation (± 1 s.d.) (a) Modelled trend of LVBC/WVBC ratio in Global area. (b-f) Modelled trend of the LVBC/WVBC ratio in different hydrological regions (Figure 1).

549 **4 Discussions and conclusion**

550 To understand the response of carbon storage potential and its inner biomass carbon stocks to
551 environmental change, we conducted a series of factorial simulations using SEIB-DGVM V3.02. More
552 importantly, we investigated the extent of the responses of carbon stocks to water limitations.

553

554 Over the past 100 years, there has been an ongoing increase in the carbon storage capacity of the
555 terrestrial ecosystem from 735 Pg C in 1916 to 855 Pg C in 2015 (Figure 6), which has slowed the rate
556 at which atmospheric CO₂ has increased and may have mitigated global warming. These findings are
557 consistent with the conclusions of research conducted at the local scale. For example, based on carbon
558 flux data, Erb et al. (2008) suggested that the vegetation carbon stock in Austria increased from 1043 Mt
559 C to 1249 Mt C (aboveground carbon stocks growth was 1.059 Mt C yr⁻¹ and belowground carbon stocks
560 growth was 0.2 Mt C yr⁻¹) since industrialization. Le Noë et al. (2020) showed that increases in the
561 carbon stocks and carbon density were the predominant drivers in the forest terrestrial carbon
562 sequestration capacity in France from 1850 to 2015. Tong et al. (2020) also found a substantial increase
563 of aboveground carbon stocks in southern China (0.11 Pg C yr⁻¹) during the period 2002–2017. However,
564 these studies focused on zonal trends in total vegetation carbon stocks and did not investigate the extent
565 of the response in vegetation carbon stocks partitioned between light- and water-gathering biomass. Our
566 results show that the increase in carbon stock in light-gathering vegetation organs was much larger than
567 that in water-gathering vegetation organs, and light-gathering biomass carbon stock dominates the
568 historical trend of the terrestrial carbon stock. During the past decades, the global land surface has been
569 greening because of the flux and storage of more carbon into plant trunks and foliage (Zhu et al., 2016).

570 LVBC increases 116.18 ± 2.34 Pg C from 1916 to 2015, accounting for 97.42% of the total carbon stock
571 increase (119.26 ± 2.44 Pg C). The long-term trends and spatial pattern of vegetation carbon stock are
572 predominated the variability characteristic of LVBC. Compared with WVBC, LVBC increase $116.18 \pm$

573 ~~2.34 Pg C and dominates the long term trends of vegetation carbon stock.~~ The latitudinal bands of
574 increasing annual change in LVBC are mainly distributed in tropical latitudes, a conclusion consistent
575 with prior knowledge that tropical zones dominate carbon uptake and storage (Erb et al., 2018; Schimel
576 et al., 2015). Under the influences of environmental stressors, WVBC increases significantly in boreal
577 latitudes. Biomass carbon allocation between light- and water-gathering vegetation organs reflect the
578 changes in individual growth, community structure and ecosystem function, which are important
579 attributes in the investigation of carbon stocks and carbon cycling within the terrestrial biosphere
580 (Hovenden et al., 2014; Fang et al., 2010; Ma et al., 2021). During the past hundred years, the ratio of
581 LVBC/WVBC ~~shown~~ showed a slight upward trend since LVBC increased more dramatically than
582 WVBC. ~~—~~The rate of increase is 0.0171 yr^{-1} , which is significant at the 0.01 level. To better absorb CO_2
583 and sunlight required for photosynthesis, vegetated regions are gradually covered by vegetation with
584 higher plant height and wider leaf area, thereby adjusting their characteristic ecosystem functions (Erb
585 et al., 2008~~Anderson et al., 2010~~).

586

587 Based on our factorial simulations (Figure 8), the influences of CO_2 fertilization induce the most
588 significant variation of the vegetation carbon stock. In addition, the responses of carbon stocks to the
589 changes of climatic factors are obvious, particularly at the zonal scale. ~~Based on our factorial simulations,~~
590 ~~the vegetation carbon stock exhibited the most increase under the influence of CO_2 fertilization. In~~
591 ~~addition, the responses of carbon stocks to climatic factors of change differed, particularly at the zonal~~
592 ~~scale (Figure 8).~~ Previous studies have pointed out that the variation of the terrestrial carbon stock caused
593 by releasing or sequestering carbon is sensitive to anomalous changes in water availability and light use
594 efficiency (Madani et al., 2020; Humphrey et al., 2018). At the grid cell scale, shown in Figure 8b and
595 8d, radiation and precipitation dominate the long-term trend of carbon stocks over one third of global
596 grid cells. At the global scale, radiation and precipitation explain approximately 10% of long-term trend
597 in LVBC and WVBC (Figure 8a and 8c). ~~At local scale, radiation dominated the long-term trend of~~
598 ~~LVBC in 20.67% of global zones and that of WVBC in 13.74%, while precipitation dominated the long-~~
599 ~~term trend of LVBC in 21.88% of global zones and that of WVBC in 17.09% of global zones. However,~~
600 ~~radiation induced light variation in LVBC (3.19%) and WVBC (5.62%) at global scale. Precipitation~~
601 ~~explain 8.51% of LVBC trend and 2.76% of WVBC trend at global scale.~~ LVBC and WVBC variations

602 driven by precipitation and radiation ~~were-are~~ ultimately offset by spatially compensatory effects, which
603 ~~dampened~~dampens the response of the carbon stock to these factors at global scale (Jung et al., 2017).
604 This spatially compensatory effect of climate changes is consistent with previous analyses (Zhu et al.,
605 2016) that climate changes explain 8% of the increasing carbon storage of global foliage, while climate
606 changes dominate the greening trend over 28.4% of the global land. Results reveal that T~~trends~~s in
607 temperature drove historical long-term trends in the potential carbon stocks, with faster increases and
608 considerable variation occurring by zone. The accumulated influence of climate warming induces
609 dramatic changes in the carbon stock at a global scale. Thus, ~~our results revealed~~ we suggest that
610 temperature dominates the long-term trends in the carbon stock among climatic drivers, while a
611 compensatory effect exists in the global change in the carbon stock induced by precipitation and radiation.
612
613 By partitioning the trends of LVBC and WVBC into five hydrological regions (Figure 1), we found that
614 the long-term change in carbon stocks is tightly coupled to terrestrial water availability. These results
615 indicate that vegetation in humid regions is responsible for most of the trend in global LVBC, while
616 plants in semi-arid regions play a dominate global role in controlling the long-term trend in WVBC
617 (Figures 9 and 10). As water stress decreases, the magnitude and range in variation of LVBC gradually
618 increase (Figure 9), which suggests that limited water availability constrains the response magnitude of
619 the changes in LVBC to changes in CO₂ and climate. The response pattern of WVBC growth to the
620 increasing water availability is different from that of LVBC. Drought mitigation promotes the growth of
621 WVBC. In sub-humid and humid regions, plants face intensified light-competition and have to invest as
622 much non-structural carbon as possible into leaf and trunk. This allocation scheme leads to the decreased
623 investment of Δ WVBC in wet regions.~~Drought mitigation promotes the growth of WVBC, while humid~~
624 ~~region with high light competition limits root growth.~~ —The result is consistent with previous finding
625 that plants reduce ~~allocation~~investment —to roots in dense forests where aboveground competition for
626 light is high (Ma et al. 2021). Moreover, we found that indirect effects of water limitation regulate
627 increasing rate of each carbon pool. Although vegetation carbon stocks dramatically increase under the
628 effects of climate and CO₂ changes, the increasing rate of LVBC faster than WVBC in humid regions .
629 Vegetation stores more biomass in aboveground plant organs (trunk and foliage) to gather light. Dryland
630 ~~vegetation-plants~~ decrease the LVBC/WVBC ratios and stores ~~s~~ more biomass below ground to enhance

631 the capture of water resources. Based on these results, we demonstrated that water limitations controlled
632 the variable response of terrestrial vegetation carbon stocks.

633

634 Our findings are consistent with other reports about the impact of increasing water limitations on
635 terrestrial ecosystem. Based on satellite remote sensing observations, Madani et al. (2020) found that
636 changes in water constraints significantly affect the response patterns of ecosystem productivity and net
637 carbon exchange, can lead to variable responses in ecosystem productivity and net carbon exchange.

638 Humphrey et al. (2021) found that increasing water stress limits the response magnitude of carbon uptake
639 rates through a down-regulation of stomatal conductance and suggested that land carbon uptake is driven
640 by temperature and vapour pressure deficit effects that are controlled by terrestrial water availability. Ma
641 et al. (2021) found that plants increase investment into building roots in arid region because the extent
642 of water limitation there is exacerbated by global warming. Terrestrial hydrological conditions
643 significantly affect the carbon cycle process of terrestrial ecosystem, including carbon uptake, allocation,
644 and stock. Terrestrial ecosystems utilize sensitive strategies to allocate and store biomass to adjust to
645 local hydrological conditions. A significant conclusion is that water constraints not only confine the
646 responses of vegetation carbon stocks to drivers of variability, but also constrain the proportion of
647 biomass carbon stocks in gather- and water-gathering fractions.

648

649 Distinguishing the response of carbon stock fractions estimated by SEIB-DGVM improves the
650 understanding of the interactive impacts of terrestrial carbon and water dynamics. However, uncertainty
651 still exists because of the limitations in the processes of modelling vegetation metabolism with SEIB-
652 DGVM. Trunk biomass contains tree branches and structural roots (coarse roots and tap roots) (Sato et
653 al., 2007), so the R/S ratio of potential vegetation in factorial simulations is smaller than the R/S of actual
654 vegetation in observation stations. Root biomass only contains the fine root biomass, leading to an
655 apparent underestimate in belowground organ biomass of trees and grasses compare with previous
656 conclusion (Ma et al., 2021; Yang et al., 2009). Availability of nitrogen is a key limiting factor for
657 vegetation growth, especially when higher CO₂ fertilization effects exist (Tharammal et al., 2019). The
658 limitation could be alleviated by nitrogen deposition in most temperate and boreal ecosystems. The
659 SEIB-DGVM experiments were conducted with a focus on documenting CO₂ fertilization and climate

660 change interactions; these experiments did not consider the influences of nitrogen deposition, which leads
661 to a slight ~~overestimate~~underestimate of the contributions of CO₂ fertilization on biomass production.–

662

663 In summary, we evaluated SEIB-DGVM V3.02 and used this model to offer new perspectives on the
664 response of vegetation carbon storage potential to changes in climate and CO₂. Our simulation results
665 show that changes in CO₂, rather than climate, dominate the light- ~~to~~and water-gathering partitioning of
666 the carbon storage potential. More importantly, we suggest that the impact of CO₂ fertilization and
667 temperature effects on vegetation carbon-sequestration potential depends on water availability and its
668 impacts on plant stress. With increased global warming, water limitations are expected to increasingly
669 confine global carbon sequestration and storage. Our findings highlight the need to account for terrestrial
670 water limitation effects when estimating the response of the terrestrial carbon storage capacity to global
671 climate change, and the need for stronger interactions between those involved in vegetation model
672 development and those in between the hydrological and ecological research communities.

674 **Table A1. MCD12C1 legend and class descriptions**

Name	Value	Description
Evergreen Needleleaf Forests	1	Dominated by evergreen conifer trees (canopy >2m). Tree cover >60%.
Evergreen Broadleaf Forests	2	Dominated by evergreen broadleaf and palmate trees (canopy >2m). Tree cover >60%.
Deciduous Needleleaf Forests	3	Dominated by deciduous needleleaf (larch) trees (canopy >2m). Tree cover >60%.
Deciduous Broadleaf Forests	4	Dominated by deciduous broadleaf trees (canopy >2m). Tree cover >60%.
Mixed Forests	5	Dominated by neither deciduous nor evergreen (40-60% of each) tree type (canopy >2m). Tree cover >60%.
Closed Shrublands	6	Dominated by woody perennials (1-2m height) >60% cover.
Open Shrublands	7	Dominated by woody perennials (1-2m height) 10-60% cover.
Woody Savannas	8	Tree cover 30-60% (canopy >2m).
Savannas	9	Tree cover 10-30% (canopy >2m).
Grasslands	10	Dominated by herbaceous annuals (<2m).
Permanent Wetlands	11	Permanently inundated lands with 30-60% water cover and >10% vegetated cover.
Croplands	12	At least 60% of area is cultivated cropland.
Urban and Built-up Lands	13	At least 30% impervious surface area including building materials, asphalt, and vehicles.
Cropland/Natural Vegetation Mosaics	14	Mosaics of small-scale cultivation 40-60% with natural tree, shrub, or herbaceous vegetation.
Permanent Snow and Ice	15	At least 60% of area is covered by snow and ice for at least 10 months of the year.
Barren	16	At least 60% of area is non-vegetated barren (sand, rock, soil) areas with less than 10% vegetation.
Water Bodies	17	At least 60% of area is covered by permanent water bodies.
Unclassified	255	Has not received a map label because of missing inputs

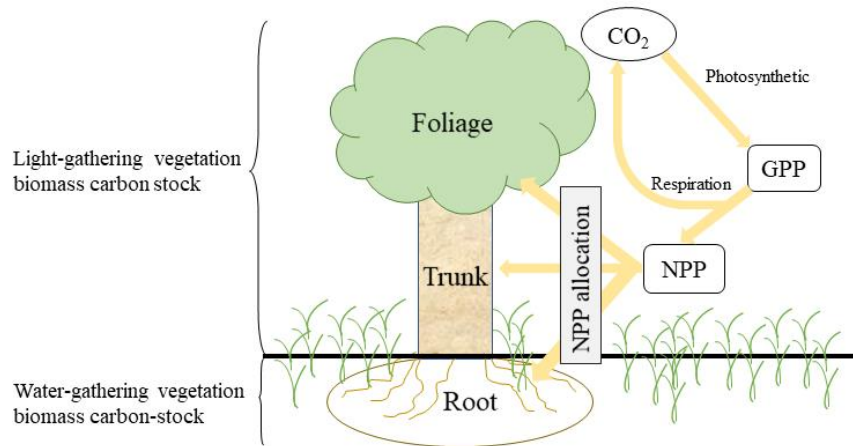


Figure A1. Schematic of ecosystem carbon cycle. Yellow arrow indicates carbon flux. Atmospheric CO₂ transitions into gross primary production (GPP) by photosynthesis. GPP is partitioned into respiration and net primary production (NPP). NPP is partitioned into three biomass carbon pools (foliage, trunk, and root).

676

677

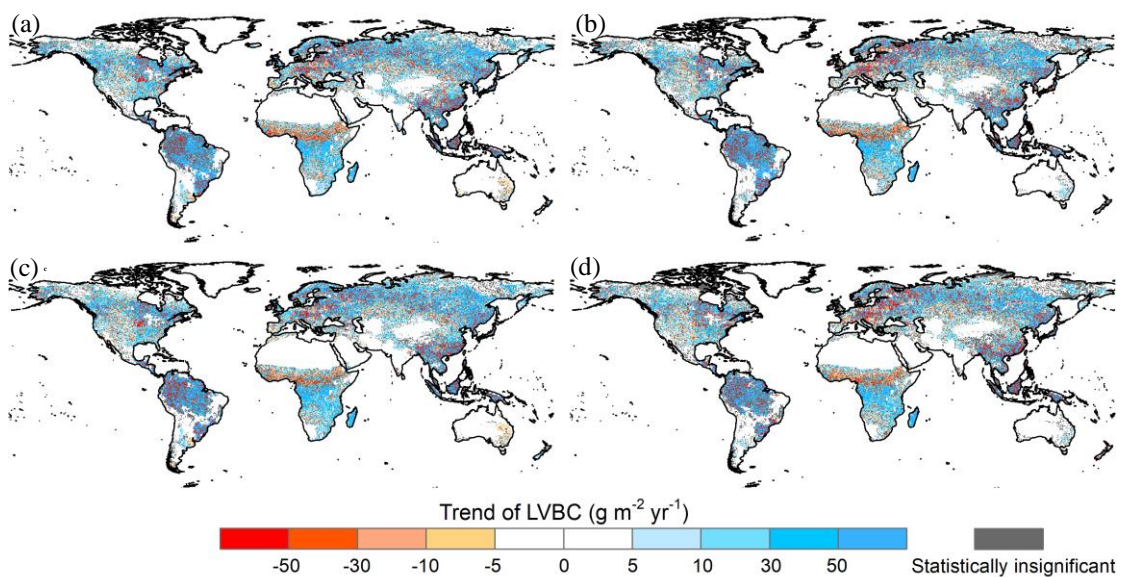


Figure A2. Potential LVBC trend maps during the period of 1916 to 2015 under different factorial simulations. (a) CO₂ driving factorial simulation (S2); (b) CO₂+precipitation driving factorial simulation (S3); (c) CO₂+temperature driving factorial simulation (S4); and (d) CO₂+radiation driving factorial simulation (S5). Positive values indicate increasing trends in the ratio, and vice versa. All results from Mann-Kendall and Sen's slope statistical tests correspond to the 95% confidence interval.

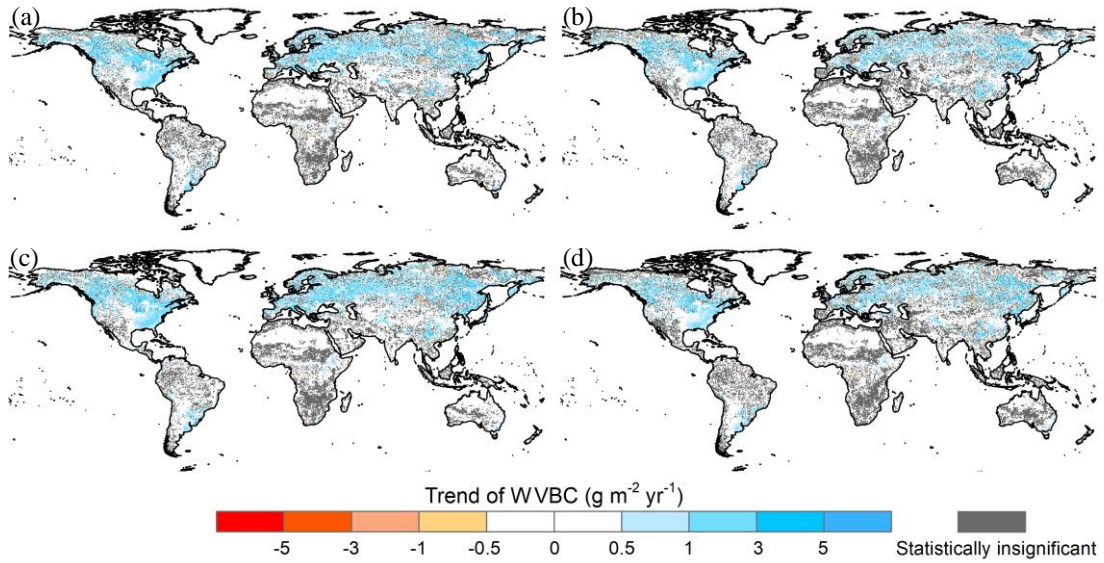


Figure A3. Potential WVBC variation trend maps during the period of 1916 to 2015 under different factorial simulations. (a) CO₂ driving factorial simulation (S2); (b) CO₂+precipitation driving factorial simulation (S3); (c) CO₂+temperature driving factorial simulation (S4); and (d) CO₂+radiation driving factorial simulation (S5). Positive values indicate increasing trends in the ratio, and vice versa. All results from Mann-Kendall and Sen's slope statistical tests correspond to the 95% confidence interval.

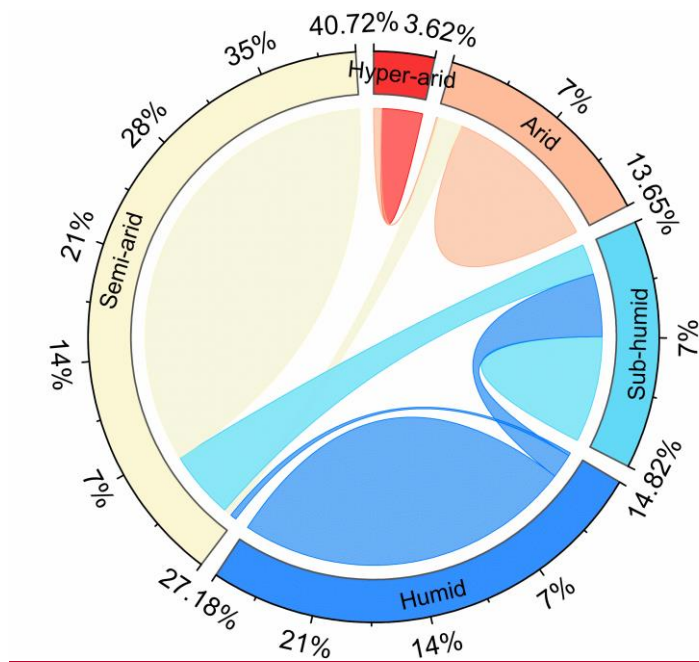


Figure A4. The shift of hydrological regions defined by the multiyear average AI index from the period

of 1916-1945 to the period of 1986-2015. The outermost number represent the percentage of hydrological regions in 1916-1945.

680

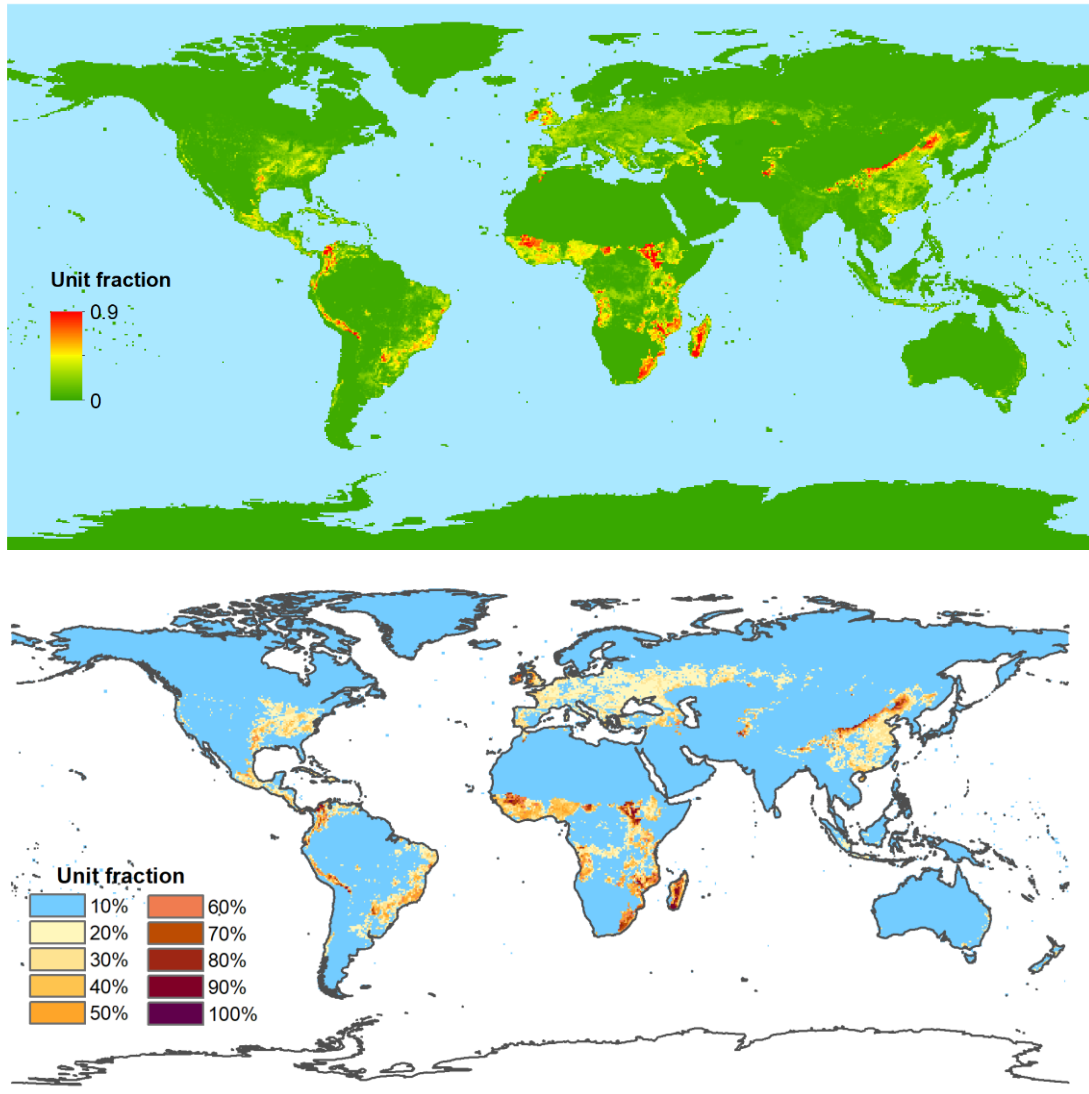


Figure A4A5. Spatial distribution of multi-year average fraction of managed pasture from 2001-2015 at 0.5×0.5 arc-degree resolution.

681

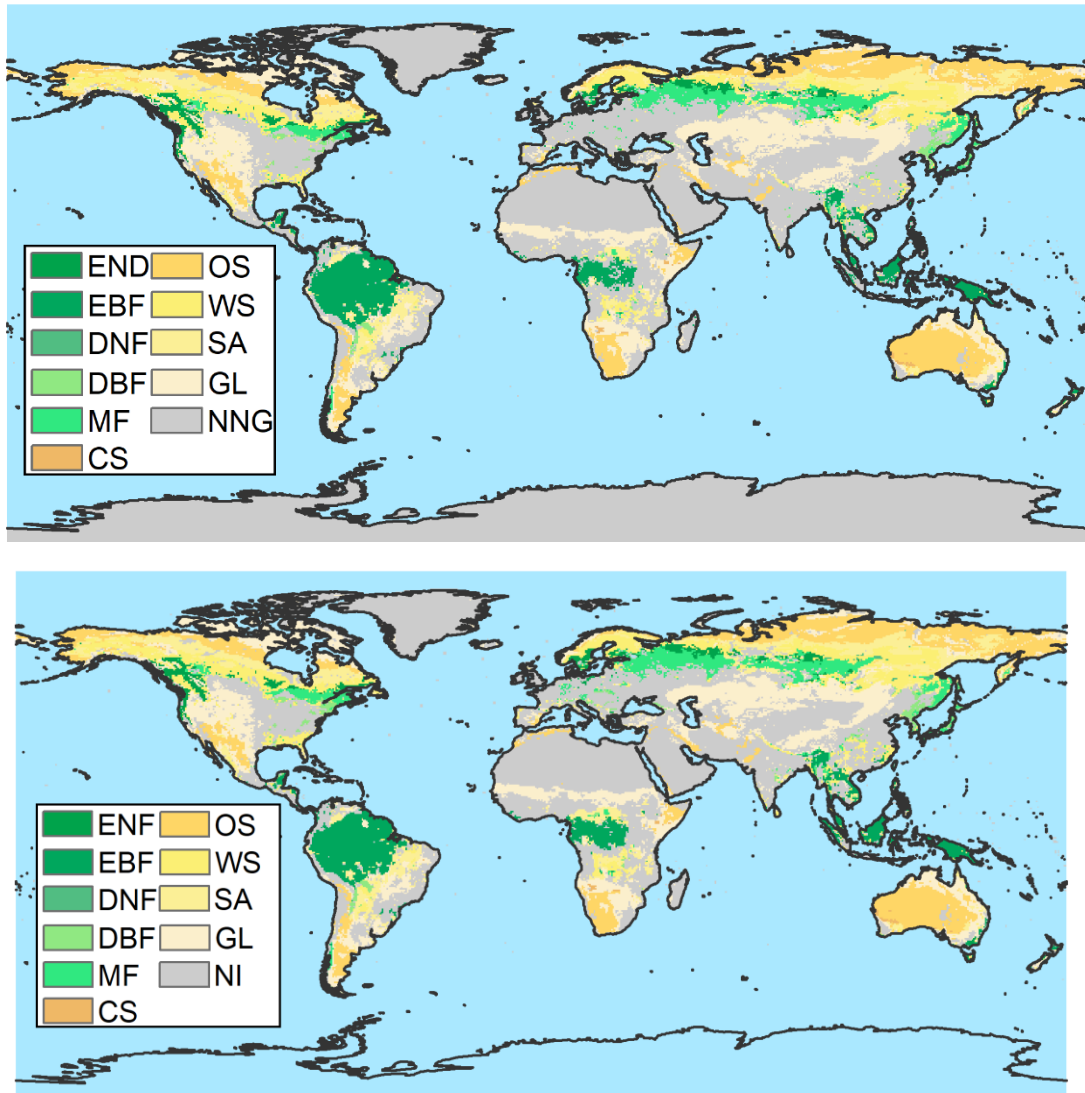


Figure A5A6. Map of land vegetation without anthropogenic disturbance from MCD12C1 and LUH2. **ENDE**: Evergreen needleleaf forest, EBF: Evergreen broadleaf forest, DNF: Deciduous needleleaf forest, DBF: Deciduous broadleaf forest, MF: Mixed forest, CS: Closed shrublands, OS: Open shrublands, WS: Woody savannas, SA: Savannas, GL: Grasslands, **NNGI**: **Not natural vegetation included**, which means the zone is not covered by vegetation without anthropogenic disturbance.

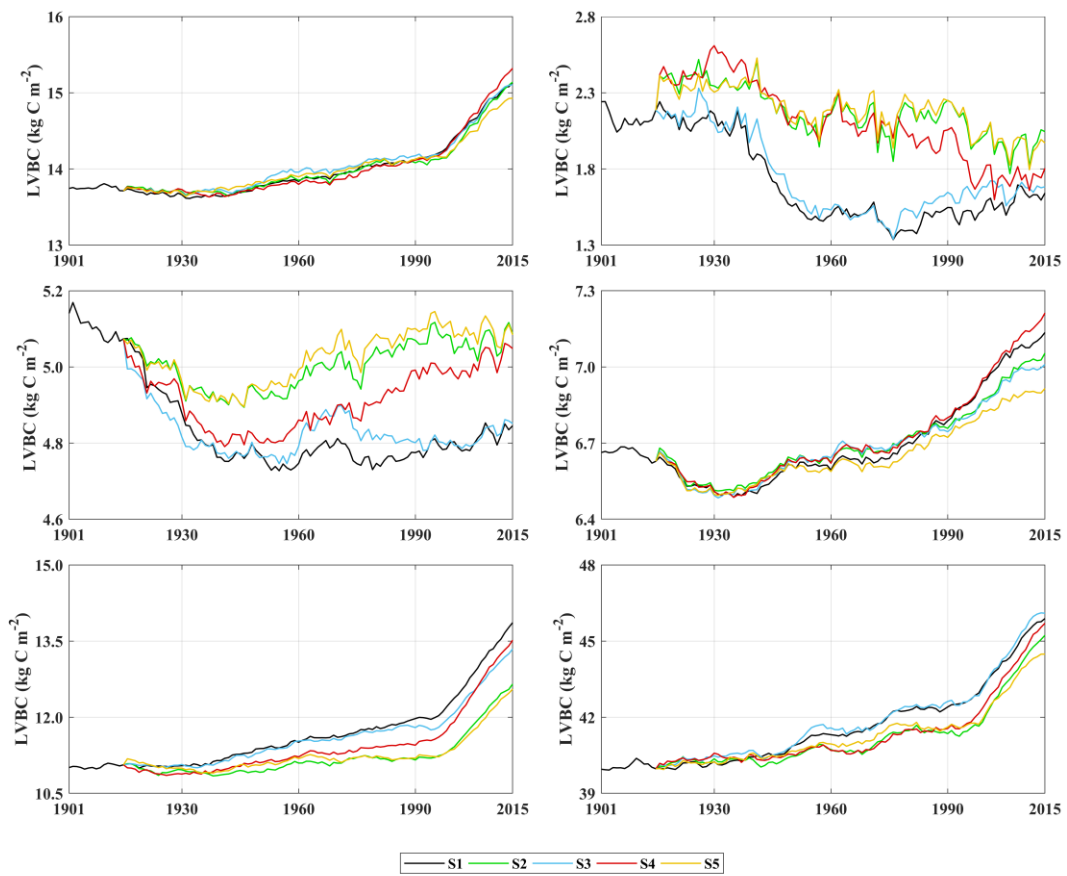
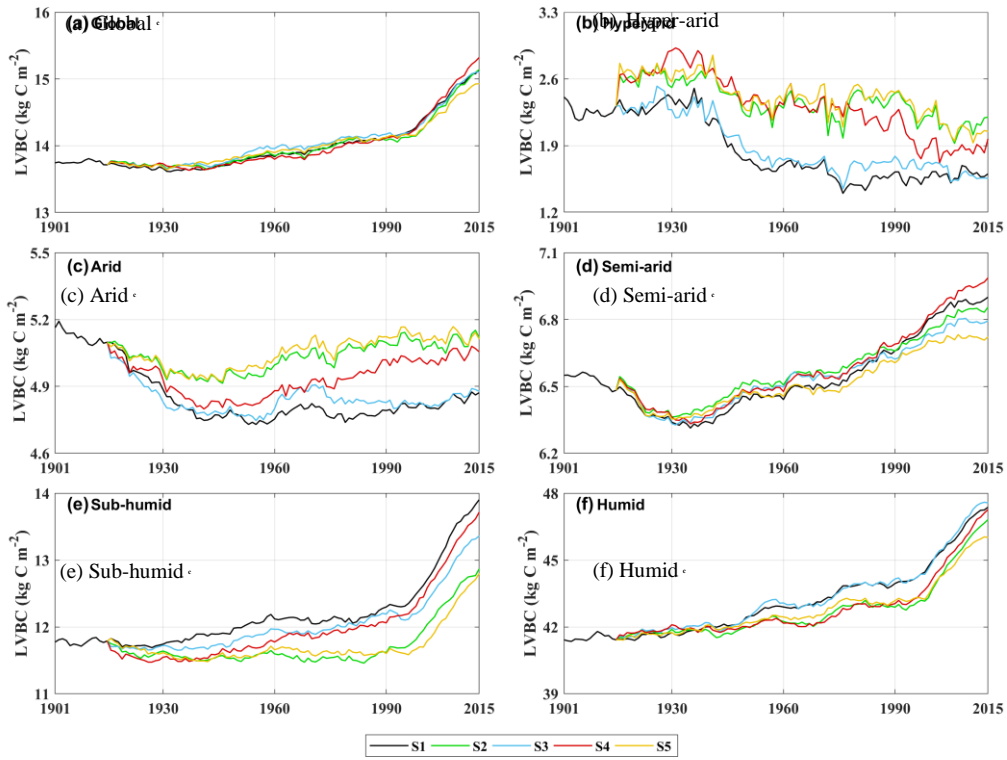
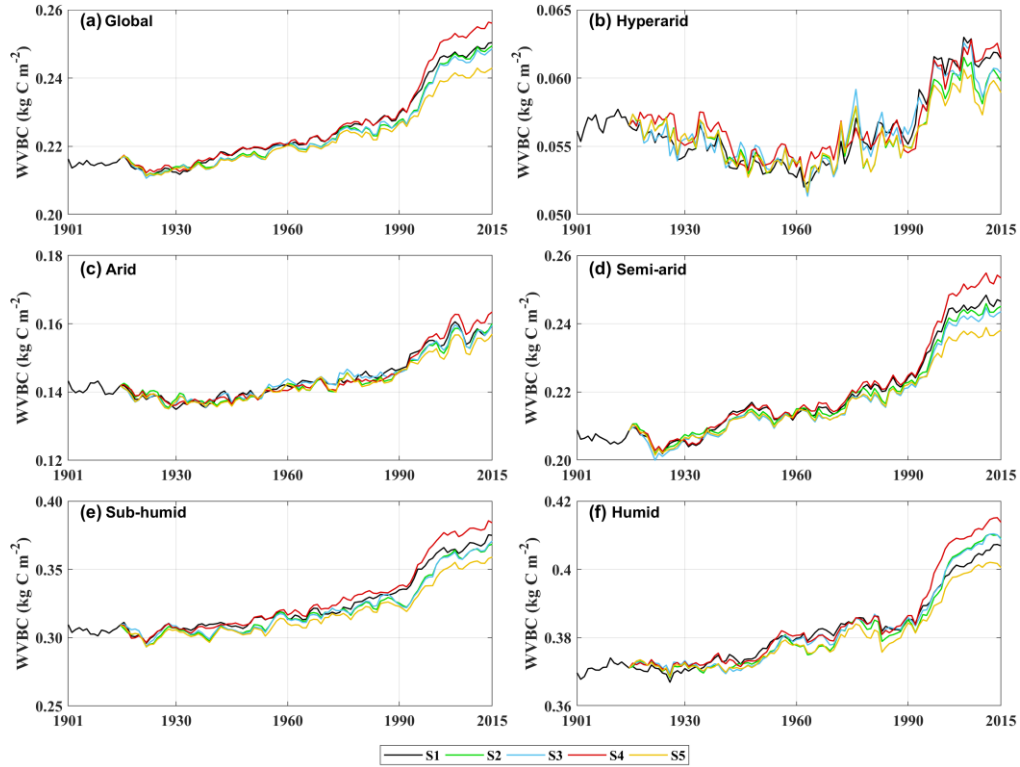


Figure A6A7. Trends in average density of potential LVBC. (a) Modelled trend of annual averaged

LVBC globally. Modelled trends in annual averaged LVBC in hyper-arid zone (b), arid zone (c), semi-arid zone (d), sub-humid zone (e), and humid zone (f).

683



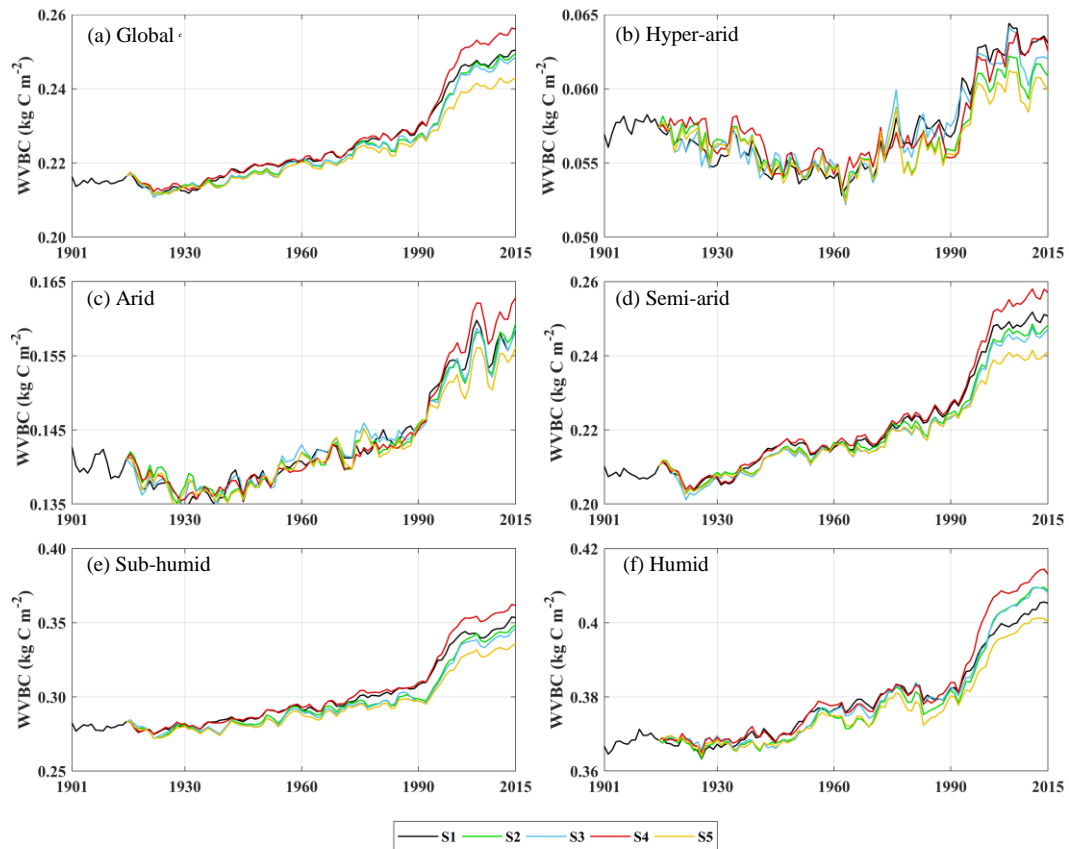


Figure A87. Trends in average density of potential WVBC. (a) Modelled trend of annual averaged WVBC globally. Modelled trends in annual averaged WVBC in hyper-arid zone (b), arid zone (c), semi-arid zone (d), sub-humid zone (e), and humid zone (f).

684 **Code and data availability statement**

685 The code of SEIB-DGVM version 3.02 can be download from <http://seib-dgvm.com/>. Climatic Research
 686 Unit data can be downloaded from <https://crudata.uea.ac.uk/cru/data/hrg/>. The soil physical parameters
 687 can be downloaded from www.iges.org/gswp. The reconstructed CO₂ concentration dataset and SEIB
 688 code can be downloaded from <http://seib-dgvm.com/>. In model validation, Ecosystem Model-Data
 689 Intercomparison (multiyear average NPP product) data were collected from
 690 https://daac.ornl.gov/NPP/guides/NPP_EMDI.html. Remote sensing product MOD17A3 data were
 691 obtained from <https://lpdaac.usgs.gov/products/mod17a3hgf006/>, MCD12C1 data were obtained from
 692 <https://ladsweb.modaps.eosdis.nasa.gov/search/order>, and LUH2 data were obtained from
 693 <https://luh.umd.edu/>.

694 **Authors contributions**

695 T.S. designed research. T.S., and S.H. performed research and developed the methodology. T.S. analyzed
696 data and produced the outputs. T.S., S.H., C.J., and X.C. wrote the first manuscript draft. W.W. and W.G.
697 supervised the study. All the authors discussed the methodology and commented on various versions of
698 the manuscript.

699 **Competing interests**

700 The authors declare that they have no conflict of interest.

701 **Acknowledgments**

702 This work was jointly supported by the National Natural Science Foundation of China (Grant Nos.
703 51979071, 51779073, 91547205), the National Key Research and Development Program of China
704 (2021YFC3201100), the Distinguished Young Fund Project of Natural Science Foundation of Jiangsu
705 Province (BK20180021), and the National “Ten Thousand Program” Youth Talent. We thank Zefeng
706 Chen for technical support. We gratefully thank the following data providers and model developers for
707 their continuous efforts and for sharing their data: the University of East Anglia, the National Centers for
708 Environmental Prediction (NCEP), the National Oceanic and Atmospheric Administration (NOAA),
709 University of Maryland, and the Center for Ocean-Land-Atmosphere Studies (COLA). Cordial thanks
710 are extended to the editor, Dr. Hans Verbeeck, and two anonymous referees for the valuable comments
711 which greatly improve the quality of the paper.

712 **References**

- 713 Ahlstrom, A., Raupach, M. R., Schurgers, G., Smith, B., Arneeth, A., Jung, M., Reichstein, M., Canadell,
 714 J. G., Friedlingstein, P., Jain, A. K., Kato, E., Poulter, B., Sitch, S., Stocker, B. D., Viovy, N., Wang,
 715 Y. P., Wiltshire, A., Zaehle, S., and Zeng, N.: The dominant role of semi-arid ecosystems in the
 716 trend and variability of the land CO₂ sink, *Science*, 348, 895-899, 10.1126/science.aaa1668, 2015.
- 717 Ajtay, G. L., Ketner, P., and Duvigneaud, P.: Terrestrial primary production and phytomass In: *The*
 718 *Global Cycle.*, Glob. Carbon Cycle, SCOPE, 129-181 pp.1979.
- 719 [Anderson, L. J., Derner, J. D., Polley, H. W., Gordon, W. S., Eissenstat, D. M., and Jackson, R. B.: Root](#)
 720 [responses along a subambient to elevated CO₂ gradient in a C3-C4 grassland, *Global Change Biol.*](#)
 721 [16, 454-468, 10.1111/j.1365-2486.2009.01975.x, 2010.](#)
- 722 Bartholome, E. and Belward, A. S.: GLC2000: a new approach to global land cover mapping from Earth
 723 observation data, *Int J Remote Sens*, 26, 1959-1977, 10.1080/01431160412331291297, 2005.
- 724 Bayer, A. D., Pugh, T. A. M., Krause, A., and Arneeth, A.: Historical and future quantification of
 725 terrestrial carbon sequestration from a Greenhouse-Gas-Value perspective, *Global Environmental*
 726 *Change*, 32, 153-164, 10.1016/j.gloenvcha.2015.03.004, 2015.
- 727 Bazilevich, N. I., Rodin, L. Y., and Rozov, N. N.: Geographical Aspects of Biological Productivity,
 728 *Soviet Geography Review and Translation*, 5, 293-317 pp.1971.
- 729 Bloom, A. A., Exbrayat, J. F., van der Velde, I. R., Feng, L., and Williams, M.: The decadal state of the
 730 terrestrial carbon cycle: Global retrievals of terrestrial carbon allocation, pools, and residence times,
 731 *Proceedings of the National Academy of Sciences of the United States of America*, 113, 1285-1290,
 732 10.1073/pnas.1515160113, 2016.
- 733 Chen, J., Ju, W., Ciais, P., Viovy, N., Liu, R. G., Liu, Y., and Lu, X. H.: Vegetation structural change
 734 since 1981 significantly enhanced the terrestrial carbon sink, *Nat Commun*, 10, 4259,
 735 10.1038/S41467-019-12257-8, 2019.
- 736 Chen, L.-P., Zhao, N.-X., Zhang, L.-H., and Gao, Y.-B.: Responses of two dominant plant species to
 737 drought stress and defoliation in the Inner Mongolia Steppe of China, *Plant Ecology*, 214, 221-229,
 738 10.1007/s11258-012-0161-y, 2013.
- 739 Cheng, L., Zhang, L., Wang, Y. P., Canadell, J. G., Chiew, F. H. S., Beringer, J., Li, L. H., Miralles, D.
 740 G., Piao, S. L., and Zhang, Y. Q.: Recent increases in terrestrial carbon uptake at little cost to the
 741 water cycle, *Nat Commun*, 8, 10.1038/s41467-017-00114-5, 2017.
- 742 Erb, K.-H., Gingrich, S., Krausmann, F., and Haberl, H.: Industrialization, Fossil Fuels, and the
 743 Transformation of Land Use, *Journal of Industrial Ecology*, 12, 686-703, 10.1111/j.1530-
 744 9290.2008.00076.x, 2008.
- 745 Erb, K.-H., Gaube, V., Krausmann, F., Plutzar, C., Bondeau, A., and Haberl, H.: A comprehensive global
 746 5min resolution land-use data set for the year 2000 consistent with national census data, *Journal of*
 747 *Land Use Science*, 2, 191-224, 10.1080/17474230701622981, 2007.
- 748 Erb, K.-H., Fetzel, T., Plutzar, C., Kastner, T., Lauk, C., Mayer, A., Niedertscheider, M., Körner, C., and
 749 Haberl, H.: Biomass turnover time in terrestrial ecosystems halved by land use, *Nat Geosci*, 9, 674-
 750 678, 10.1038/ngeo2782, 2016.
- 751 Erb, K.-H., Kastner, T., Plutzar, C., Bais, A. L. S., Carvalhais, N., Fetzel, T., Gingrich, S., Haberl, H.,
 752 Lauk, C., Niedertscheider, M., Pongratz, J., Thurner, M., and Luyssaert, S.: Unexpectedly large
 753 impact of forest management and grazing on global vegetation biomass, *Nature*, 553, 73-76,
 754 10.1038/nature25138, 2018.

755 Fan, L., Wigneron, J. P., Ciais, P., Chave, J., Brandt, M., Fensholt, R., Saatchi, S. S., Bastos, A., Al-
756 Yaari, A., Hufkens, K., Qin, Y. W., Xiao, X. M., Chen, C., Myneni, R. B., Fernandez-Moran, R.,
757 Mialon, A., Rodriguez-Fernandez, N. J., Kerr, Y., Tian, F., and Penuelas, J.: Satellite-observed
758 pantropical carbon dynamics, *Nat Plants*, 5, 944-951, 10.1038/s41477-019-0478-9, 2019.

759 Fang, J., Yang, Y., Ma, W., Mohammat, A., and Shen, H.: Ecosystem carbon stocks and their changes
760 in China's grasslands, *Science China. Life sciences*, 53, 757-765, 10.1007/s11427-010-4029-x, 2010.

761 Friedlingstein, P., Joel, G., Field, C. B., and Fung, I. Y.: Toward an allocation scheme for global
762 terrestrial carbon models, *Global Change Biol*, 5, 755-770, DOI 10.1046/j.1365-2486.1999.00269.x,
763 1999.

764 Gentine, P., Green, J. K., Guérin, M., Humphrey, V., Seneviratne, S. I., Zhang, Y., and Zhou, S.:
765 Coupling between the terrestrial carbon and water cycles—a review, *Environ Res Lett*, 14, 083003,
766 10.1088/1748-9326/ab22d6, 2019.

767 Gill, R. and Jackson, R.: Global patterns of root turnover for terrestrial ecosystems, *New Phytol*, 147,
768 13-31, 10.1046/j.1469-8137.2000.00681.x, 2000.

769 Gocic, M. and Trajkovic, S.: Analysis of changes in meteorological variables using Mann-Kendall and
770 Sen's slope estimator statistical tests in Serbia, *Global and Planetary Change*, 100, 172-182,
771 10.1016/j.gloplacha.2012.10.014, 2013.

772 Gulbeyaz, O., Bond-Lamberty, B., Akyurek, Z., and West, T. O.: A new approach to evaluate the MODIS
773 annual NPP product (MOD17A3) using forest field data from Turkey, *Int J Remote Sens*, 39, 2560-
774 2578, 10.1080/01431161.2018.1430913, 2018.

775 Haberl, H., Erb, K. H., and Krausmann, F.: Human Appropriation of Net Primary Production: Patterns,
776 Trends, and Planetary Boundaries, *Annu Rev Env Resour*, 39, 363-391, 10.1146/annurev-environ-
777 121912-094620, 2014.

778 Harper, A. B., Wiltshire, A. J., Cox, P. M., Friedlingstein, P., Jones, C. D., Mercado, L. M., Sitch, S.,
779 Williams, K., and Duran-Rojas, C.: Vegetation distribution and terrestrial carbon cycle in a carbon
780 cycle configuration of JULES4.6 with new plant functional types, *Geosci Model Dev*, 11, 2857-
781 2873, 10.5194/gmd-11-2857-2018, 2018.

782 Harris, I., Osborn, T. J., Jones, P., and Lister, D.: Version 4 of the CRU TS monthly high-resolution
783 gridded multivariate climate dataset, *Scientific Data*, 7, 109, 10.1038/s41597-020-0453-3, 2020.

784 Hovenden, M. J., Newton, P. C., and Wills, K. E.: Seasonal not annual rainfall determines grassland
785 biomass response to carbon dioxide, *Nature*, 511, 583-586, 10.1038/nature13281, 2014.

786 Humphrey, V., Zscheischler, J., Ciais, P., Gudmundsson, L., Sitch, S., and Seneviratne, S. I.: Sensitivity
787 of atmospheric CO₂ growth rate to observed changes in terrestrial water storage, *Nature*, 560, 628-
788 631, 10.1038/s41586-018-0424-4, 2018.

789 Humphrey, V., Berg, A., Ciais, P., Gentine, P., Jung, M., Reichstein, M., Seneviratne, S. I., and
790 Frankenberg, C.: Soil moisture–atmosphere feedback dominates land carbon uptake variability,
791 *Nature*, 592, 65-69, 10.1038/s41586-021-03325-5, 2021.

792 Hurtt, G. C., Chini, L. P., Frolking, S., Betts, R. A., Feddema, J., Fischer, G., Fisk, J. P., Hibbard, K.,
793 Houghton, R. A., Janetos, A., Jones, C. D., Kindermann, G., Kinoshita, T., Goldewijk, K. K., Riahi,
794 K., Shevliakova, E., Smith, S., Stehfest, E., Thomson, A., Thornton, P., van Vuuren, D. P., and
795 Wang, Y. P.: Harmonization of land-use scenarios for the period 1500-2100: 600 years of global
796 gridded annual land-use transitions, wood harvest, and resulting secondary lands, *Climate Change*,
797 109, 117-161, 10.1007/s10584-011-0153-2, 2011.

798 Hurtt, G. C., Chini, L., Sahajpal, R., Frolking, S., Bodirsky, B. L., Calvin, K., Doelman, J. C., Fisk, J.,

799 Fujimori, S., Goldewijk, K. K., Hasegawa, T., Havlik, P., Heinemann, A., Humpenöder, F.,
800 Jungclauss, J., Jed Kaplan, Kennedy, J., Kristzin, T., Lawrence, D., Lawrence, P., Ma, L., Mertz, O.,
801 Pongratz, J., Popp, A., Poulter, B., Riahi, K., Shevliakova, E., Stehfest, E., Thornton, P., Tubiello,
802 F. N., van Vuuren, D. P., Zhang, X.: Harmonization of Global Land-Use Change and Management
803 for the Period 850-2100 (LUH2) for CMIP6, *Geoscientific Model Development*, 13, 5425-5464,
804 10.5194/gmd-13-5425-2020, 2021.

805 IPCC: Impacts, Adaptation and Vulnerability. Contribution of Working Group II to the Fourth
806 Assessment Report of the Intergovernmental Panel on Climate Change, - 2007.

807 Jung, M., Reichstein, M., Schwalm, C. R., Huntingford, C., Sitch, S., Ahlstrom, A., Arneeth, A., Camps-
808 Valls, G., Ciais, P., Friedlingstein, P., Gans, F., Ichii, K., Jain, A. K., Kato, E., Papale, D., Poulter,
809 B., Raduly, B., Rodenbeck, C., Tramontana, G., Viovy, N., Wang, Y. P., Weber, U., Zaehle, S., and
810 Zeng, N.: Compensatory water effects link yearly global land CO₂ sink changes to temperature,
811 *Nature*, 541, 516-520, 10.1038/nature20780, 2017.

812 Kaplan, J. O., Krumhardt, K. M., Ellis, E. C., Ruddiman, W. F., Lemmen, C., and Goldewijk, K. K.:
813 Holocene carbon emissions as a result of anthropogenic land cover change, *Holocene*, 21, 775-791,
814 10.1177/0959683610386983, 2011.

815 Keenan, T. F., Prentice, I. C., Canadell, J. G., Williams, C. A., Wang, H., Raupach, M., and Collatz, G.
816 J.: Recent pause in the growth rate of atmospheric CO₂ due to enhanced terrestrial carbon uptake
817 *Nat Commun*, 7, 10.1038/Ncomms16137, 2017.

818 Kindermann, G. E., Mcallum, I., Fritz, S., and Obersteiner, M.: A global forest growing stock, biomass
819 and carbon map based on FAO statistics, *Silva Fenn*, 42, 387-396, 10.14214/Sf.244, 2008.

820 Le Noë, J., Matej, S., Magerl, A., Bhan, M., Erb, K. H., and Gingrich, S.: Modeling and empirical
821 validation of long-term carbon sequestration in forests (France, 1850-2015), *Glob Chang Biol*, 26,
822 2421-2434, 10.1111/gcb.15004, 2020.

823 Liu, J., Bowman, K. W., Schimel, D. S., Parazoo, N. C., Jiang, Z., Lee, M., Bloom, A. A., Wunch, D.,
824 Frankenberg, C., Sun, Y., O'Dell, C. W., Gurney, K. R., Menemenlis, D., Gierach, M., Crisp, D.,
825 and Eldering, A.: Contrasting carbon cycle responses of the tropical continents to the 2015-2016 El
826 Nino, *Science*, 358, eaam5690, 10.1126/science.aam5690, 2017.

827 Ma, H. Z., Mo, L. D., Crowther, T. W., Maynard, D. S., van den Hoogen, J., Stocker, B. D., Terrer, C.,
828 and Zohner, C. M.: The global distribution and environmental drivers of aboveground versus
829 belowground plant biomass, *Nat Ecol Evol*, 5, 1110+, 10.1038/s41559-021-01485-1, 2021.

830 Madani, N., Parazoo, N. C., Kimball, J. S., Ballantyne, A. P., Reichle, R. H., Maneta, M., Saatchi, S.,
831 Palmer, P. I., Liu, Z., and Tagesson, T.: Recent Amplified Global Gross Primary Productivity Due
832 to Temperature Increase Is Offset by Reduced Productivity Due to Water Constraints, *AGU*
833 *Advances*, 2, e2020AV000180, 10.1029/2020AV000180, 2020.

834 Magerl, A., Le Noë, J., Erb, K.-H., Bhan, M., and Gingrich, S.: A comprehensive data-based assessment
835 of forest ecosystem carbon stocks in the U.S. 1907–2012, *Environ Res Lett*, 14, 125015,
836 10.1088/1748-9326/ab5cb6, 2019.

837 McConnaughay, K. D. M. and Coleman, J. S.: Biomass allocation in plants: ontogeny or optimality? A
838 test along three resource gradients, *Ecology*, 80, 2581-2593, 10.1890/0012-
839 9658(1999)080[2581:BAIPOO]2.0.CO;2, 1999.

840 Monteith, J. L. and Unsworth, M. H.: *Principles of Environmental Physics*, 2nd ed., London 1990.

841 Olson, J., Watts, J., and Allison, L.: *Carbon in Live Vegetation of Major World Ecosystems*, Oak Ridge
842 National Laboratory 1983.

843 Pan, Y. D., Birdsey, R. A., Phillips, O. L., and Jackson, R. B.: The Structure, Distribution, and Biomass
844 of the World's Forests, *Annu Rev Ecol Evol S*, 44, 593-622, 10.1146/annurev-ecolsys-110512-
845 135914, 2013.

846 Pan, Y. D., Birdsey, R. A., Fang, J. Y., Houghton, R., Kauppi, P. E., Kurz, W. A., Phillips, O. L.,
847 Shvidenko, A., Lewis, S. L., Canadell, J. G., Ciais, P., Jackson, R. B., Pacala, S. W., McGuire, A.
848 D., Piao, S. L., Rautiainen, A., Sitch, S., and Hayes, D.: A Large and Persistent Carbon Sink in the
849 World's Forests, *Science*, 333, 988-993, 10.1126/science.1201609, 2011.

850 Piao, S. L., Friedlingstein, P., Ciais, P., Zhou, L. M., and Chen, A. P.: Effect of climate and CO₂ changes
851 on the greening of the Northern Hemisphere over the past two decades, *Geophys Res Lett*, 33,
852 L23402, 10.1029/2006GL028205, 2006.

853 Piao, S. L., Wang, X., Wang, K., Li, X., Bastos, A., Canadell, J. G., Ciais, P., Friedlingstein, P., and
854 Sitch, S.: Interannual variation of terrestrial carbon cycle: Issues and perspectives, *Glob Chang Biol*,
855 26, 300-318, 10.1111/gcb.14884, 2020.

856 Poorter, H.: Construction costs and payback time of biomass: a whole plant perspective, *A Whole-Plant
857 Perspective on Carbon-Nitrogen Interactions*, SPB Academic Publishing, The Hague 1994.

858 Poulter, B., Frank, D., Ciais, P., Myneni, R. B., Andela, N., Bi, J., Broquet, G., Canadell, J. G., Chevallier,
859 F., Liu, Y. Y., Running, S. W., Sitch, S., and van der Werf, G. R.: Contribution of semi-arid
860 ecosystems to interannual variability of the global carbon cycle, *Nature*, 509, 600-603,
861 10.1038/nature13376, 2014.

862 Prentice, I. C., Harrison, S. P., and Bartlein, P. J.: Global vegetation and terrestrial carbon cycle changes
863 after the last ice age, *New Phytol*, 189, 988-998, 10.1111/j.1469-8137.2010.03620.x, 2011.

864 Roy, J., Saugier, B., and Mooney, H. A.: Estimations of global terrestrial productivity: converging toward
865 a single number? In: *Terrestrial Global Productivity*, Academic Press, San Diego 2001.

866 Ruesch, A. and Gibbs, H. K.: New IPCC Tier-1 global biomass carbon map for the year 2000, 2008.

867 Ryan, M. G.: Effects of Climate Change on Plant Respiration, *Ecological Applications*, 1, 157-167,
868 10.2307/1941808, 1991.

869 Sato, H., Itoh, A., and Kohyama, T.: SEIB-DGVM: A new Dynamic Global Vegetation Model using a
870 spatially explicit individual-based approach, *Ecological Modelling*, 200, 279-307,
871 10.1016/j.ecolmodel.2006.09.006, 2007.

872 Sato, H., Kobayashi, H., Beer, C., and Fedorov, A.: Simulating interactions between topography,
873 permafrost, and vegetation in Siberian larch forest, *Environ Res Lett*, 15, 095006, 10.1088/1748-
874 9326/Ab9be4, 2020.

875 Saugier, B., Roy, J., and Mooney, H.: Estimations of Global Terrestrial Productivity, *Terrestrial Global
876 Productivity*, Academic Press, San Diego, Calif 2001.

877 Schimel, D., Stephens, B. B., and Fisher, J. B.: Effect of increasing CO₂ on the terrestrial carbon cycle,
878 *Proceedings of the National Academy of Sciences of the United States of America*, 112, 436-441,
879 10.1073/pnas.1407302112, 2015.

880 Seo, H. and Kim, Y.: Interactive impacts of fire and vegetation dynamics on global carbon and water
881 budget using Community Land Model version 4.5, *Geosci Model Dev*, 12, 457-472, 10.5194/gmd-
882 12-457-2019, 2019.

883 Shevliakova, E., Pacala, S. W., Malyshev, S., Hurtt, G. C., Milly, P. C. D., Caspersen, J. P., Sentman, L.
884 T., Fisk, J. P., Wirth, C., and Crevoisier, C.: Carbon cycling under 300 years of land use change:
885 Importance of the secondary vegetation sink, *Global Biogeochem Cy*, 23, 10.1029/2007gb003176,
886 2009.

887 Sun, F., Roderick, M. L., and Farquhar, G. D.: Changes in the variability of global land precipitation,
888 *Geophys Res Lett*, 39, L19402, 10.1029/2012gl053369, 2012.

889 Tei, S., Sugimoto, A., Liang, M. C., Yonenobu, H., Matsuura, Y., Osawa, A., Sato, H., Fujinuma, J., and
890 Maximov, T.: Radial Growth and Physiological Response of Coniferous Trees to Arctic
891 Amplification, *J Geophys Res-Bioge*, 122, 2786-2803, 10.1002/2016JG003745, 2017.

892 Terrer, C., Phillips, R. P., Hungate, B. A., Rosende, J., Pett-Ridge, J., Craig, M. E., van Groenigen, K. J.,
893 Keenan, T. F., Sulman, B. N., Stocker, B. D., Reich, P. B., Pellegrini, A. F. A., Pendall, E., Zhang,
894 H., Evans, R. D., Carrillo, Y., Fisher, J. B., Van Sundert, K., Vicca, S., and Jackson, R. B.: A trade-
895 off between plant and soil carbon storage under elevated CO₂, *Nature*, 591, 599-603,
896 10.1038/s41586-021-03306-8, 2021.

897 Tharammal, T., Bala, G., Devaraju, N., and Nemani, R.: A review of the major drivers of the terrestrial
898 carbon uptake: model-based assessments, consensus, and uncertainties, *Environ Res Lett*, 14,
899 093005, 10.1088/1748-9326/Ab3012, 2019.

900 Tong, X. W., Brandt, M., Yue, Y. M., Ciais, P., Jepsen, M. R., Penuelas, J., Wigner, J. P., Xiao, X.
901 M., Song, X. P., Horion, S., Rasmussen, K., Saatchi, S., Fan, L., Wang, K. L., Zhang, B., Chen, Z.
902 C., Wang, Y. H., Li, X. J., and Fensholt, R.: Forest management in southern China generates short
903 term extensive carbon sequestration, *Nat Commun*, 11, 10.1038/s41467-019-13798-8, 2020.

904 West, P. C., Gibbs, H. K., Monfreda, C., Wagner, J., Barford, C. C., Carpenter, S. R., and Foley, J. A.:
905 Trading carbon for food: Global comparison of carbon stocks vs. crop yields on agricultural land,
906 *Proceedings of the National Academy of Sciences of the United States of America*, 107, 19645-
907 19648, 10.1073/pnas.1011078107, 2010.

908 Wild, M., Gilgen, H., Roesch, A., Ohmura, A., Long, C. N., Dutton, E. G., Forgan, B., Kallis, A., Russak,
909 V., and Tsvetkov, A.: From dimming to brightening: Decadal changes in solar radiation at Earth's
910 surface, *Science*, 308, 847-850, 10.1126/science.1103215, 2005.

911 Yang, Y., Fang, J., Ma, W., Guo, D., and Mohammat, A.: Large-scale pattern of biomass partitioning
912 across China's grasslands, *Global Ecology and Biogeography*, 19, 268-277, 10.1111/j.1466-
913 8238.2009.00502.x, 2010.

914 Zhang, H., Song, T. Q., Wang, K. L., Yang, H., Yue, Y. M., Zeng, Z. X., Peng, W. X., and Zeng, F. P.:
915 Influences of stand characteristics and environmental factors on forest biomass and root-shoot
916 allocation in southwest China, *Ecol Eng*, 91, 7-15, 10.1016/j.ecoleng.2016.01.040, 2016.

917 Zhu, Z. C., Piao, S. L., Myneni, R. B., Huang, M. T., Zeng, Z. Z., Canadell, J. G., Ciais, P., Sitch, S.,
918 Friedlingstein, P., Arneeth, A., Cao, C. X., Cheng, L., Kato, E., Koven, C., Li, Y., Lian, X., Liu, Y.
919 W., Liu, R. G., Mao, J. F., Pan, Y. Z., Peng, S. S., Penuelas, J., Poulter, B., Pugh, T. A. M., Stocker,
920 B. D., Viovy, N., Wang, X. H., Wang, Y. P., Xiao, Z. Q., Yang, H., Zaehle, S., and Zeng, N.:
921 Greening of the Earth and its drivers, *Nat Clim Change*, 6, 791-+, 10.1038/Nclimate3004, 2016.